Intergalactic H I complexes without optical-counterparts in LGG 334

A. Popping
supervisors: E. Noordermeer, R. Boomsma and J.M. van der Hulst

Kapteyn Astronomical Institute, P.O. Box 800, 9700 AV Groningen, the Netherlands

Abstract. We present new observations on several wavelengths of the central part of LGG 334 which are much deeper than previous observations. The 21-cm line of neutral hydrogen is observed for 4×12 hours with the Westerbork Synthesis Radio Telescope (WSRT). At low spatial resolution ($\sim$60"), the radio data reach a limiting column density of 0.5×10^{18} cm^{-2} (1σ), while at high spatial resolution ($\sim$15"), a 1σ limiting column density of 4×10^{18} cm^{-2} is reached. Beside the known group members, eight other H I complexes are detected. Five pointings are observed in the optical R and B band with the MDM Hiltner 2.4m telescope to look for optical counterparts. For the H I complexes no optical counterparts are found to a 1σ surface brightness limit of 27.6 mag arcsec^{-2} in the B-band and 27.2 mag arcsec^{-2} in the R band. These intergalactic complexes have a filamentary structure, with dense parts. The total H I mass of the eight complexes is $\sim 2.4 \times 10^8$ M$_\odot$. In the largest H I complex, the mass is 1.28×10^8 M$_\odot$, comparable to a dwarf galaxy. In this complex the column density goes up to 6×10^{20} cm^{-2}. No physical connections can be seen between the group members, but we believe the complexes are caused by interactions of one, or more of the group members in the group center. NGC 5002 is most likely to be the putative galaxy for the intergalactic gas. The group is at a distance of 15.7 Mpc and all the H I complexes are detected within 100 kpc projected radius of the group members NGC 5002 and NGC 5014. A polar ring structure is found in NGC 5014, which is probably caused by the accretion of intergalactic gas in the same event..

Key words. galaxies: interactions – galaxies: intergalactic medium – galaxies: individual (NGC 5014) – radio lines: galaxies

1. Introduction

Massive intra-group clouds of neutral hydrogen without optical counterparts are not very common, but are known to exist in several groups; e.g., Schneider et al. (1989), Hibbard et al. (2001), Barnes & Webster (2001).
Probably the best known example of a large intergalactic H I cloud is the Leo Ring (Schneider et al., 1989). The Leo Ring is a large ring of H I gas with a diameter of approximately 200 kpc in the M96 group. The cloud has been searched for signs of emission over a wide range of frequencies, however this was not found (Schneider et al., 1989).
Several scenarios have been proposed to explain the origin of intergalactic gas clouds.
Hydrogen is the most primitive atomic element, and was first formed after the Big Bang. A question is whether there exist remnants of clouds of primordial hydrogen. This primordial matter would exist as self gravitationally bound systems in the intergalactic medium. The interpretation of Schneider et al. (1989) is that the gas in the Leo Ring has a primordial origin.
The idea of primordial gas clouds is still very controversial, the existence of these primordial H I clouds are questioned by Briggs (2005).
Some of the intergalactic gas clouds are explained by High Velocity Clouds (HVCs). HVCs were discovered by Muller et al. (1963) in the 21-cm line of neutral hydrogen. As apparent from their name, these are clouds with high radial velocities. These velocities are incompatible for participation with the rotation of our galaxy. HVCs have many forms, they can be found in the form of isolated, compact clouds, as well as extended complexes all across the sky.
The two main features of HVCs are (1) a radial velocity which is discrepant from the velocity due to Galaxy rotation in the direction of the feature and (2) no optical emission, which means no obvious stellar counterpart. This is not a very satisfactory definition of a HVC. However there is not a clear generally accepted explanation for the origin and a description of the basic parameters. This results in a very broad class, with two

Send offprint requests to: A. Popping e-mail: popping@astro.rug.nl

features and furthermore defined by what they are not.
High Velocity Clouds represent a variety of phenomena; an overview is given by Wakker & van Woerden (1997). Some possible explanations are tidal debris or infalling gas.
Analogs to the High Velocity Clouds seen around the Milky Way may exist in other groups.
Cold Dark Matter (CDM) models of structure formation predict a large population of "mini-halos" at large distances. Blitz et al. (1999) and Braun & Burton (1999) have argued that an important subset of HVCs could represent this predicted population. However there is some variation in the models of this scenario. Blitz et al. (1999) suggest that HVCs have masses of $\sim 10^7 M_\odot$ at distances of $\sim$ 1 Mpc. Braun & Burton (1999) however have stated that only Compact HVCs (CHVC) are at such large distances. Most recent models of this scenario are presented by de Heij et al. (2002) who suggested that clouds have masses of 10^5 - $10^7 M_\odot$ and sizes of $\sim$ 2 kpc, at distances within 150-200 kpc of the Milky Way. A strong test of these models would be to check, whether these clouds can be seen around other galaxies. In several nearby groups, searches are made in H I for low mass satellites to a limit of $\sim 7 \times 10^6 M_\odot$; e.g., Zwaan (2001). However in none of these searches H I rich satellites were found with very little or no optical emission. This lead to the conclusion that massive H I clouds are rare in the group environment.
Minchin et al. (2005) have very recently claimed to have found a hydrogen cloud in the Virgo Cluster with a mass of $10^8 M_\odot$, which they interpreted as a dark halo as expected by Dark Matter models.

A lot of neutral hydrogen gas is in some way linked to galaxies as a result of interactions.
In the outer parts of spiral galaxies, H I gas is very loosely bound. Therefore, in the case of interactions between spiral galaxies, the outer H I gas can easily be disturbed. This gas may be tidally driven into the centre of the galaxies, or could be rejected into tidal streams. When tidal streams collide or become compressed, the gas may be turned into stars.
Very often outlaying clouds can be explained as a result of tidal interactions, by tracing the H I distribution and kinematics back to the original galaxies and detecting connections between the clouds and the main group members. In most cases, faint optical emission can be detected in such gas filaments.
The dynamical evolution of debris is mainly governed by gravitational physics as is shown by Toomre & Toomre (1972).
The extreme version of galaxy interaction is that a galaxy is completely destroyed by another galaxy. In this case there is no merging, the material of the destroyed galaxy is spread out in such a way that the surface brightness is below the detection limit for optical observations. Only the H I remains observable (Ryan-Weber et al., 2003).
Compact groups are ideal laboratories to study the physics of interactions and mergers and the evolution of the remnants.
To investigate intergalactic structures, blind H I surveys of galaxy groups are needed, which can give unexpected results. Several examples are found of rings of gas, encircling the core of a loose group; e.g., Barnes & Webster (2001). They found a galaxy sized mass in LGG 445, where the column density exceeds the threshold density for star formation, but is still optically invisible.

Strong indications exist for intergalactic H I gas in the neighborhood of NGC 5014, a galaxy in LGG 334. The group contains 13 galaxies, of which NGC 5005 and NGC 5033 are the dominant members (Garcia, 1993).
Previous observations have shown emission of H I gas in the centre of the group. Thean et al. (1997) have reported H I emission in the group center. In a study of the Seyfert galaxy NGC 5033, they determined a H I mass of $5.7 \times 10^7 M_\odot$ next to the galaxy. Thean et al. (1997) have already mentioned that this source is not found in the UGC catalogue,
Noordermeer et al. (2005) found a more complex structure and reported a number of large H I clouds, all without optical counterparts.
Neither of the previous observations were deep, because they were not directly pointed at the intergalactic region of LGG 334. At the location of the H I emission no group members are known, so deeper observations are needed to put more constraints on this H I gas.
It is likely that group member NGC 5014 is somehow related to this H I emission. NGC 5014 is classified as an SA galaxy and was last observed in H I in a single 12 hour run in the framework of the early-type disk part of the WHISP galaxy survey (Noordermeer et al., 2005). The galaxy is one of the smaller group members in the center of LGG 334. The structure is very interesting, as well in the optical, as in H I. A DSS[1] image shows that the galaxy has a clear disk with two small extensions at both sides of the main disk. These extensions, together with a prominent dust feature perpendicular to the main disk, suggest a polar ring.
Polar ring galaxies (PRG) are peculiar systems which are made up of an early type host galaxy, surrounded by a ring of stars and gas, orbiting in a plane that is nearly polar. PRGs are interesting systems, and many studies have focused on them, because the presence of the two dynamical planes can be used to put constraints on the shape of the dark halos. Polar rings are thought to be formed during a secondary event around a preexisting galaxy. Two kind of scenarios have been proposed, the

[1] The Palomar Observatory SKY Survey was made by the California Institute of Technology with funds from the National Science Foundation, the National Geographic Society, the Sloan Foundation, the Samual Oschin Foundation, and the Eastman Kodak Corporation. The Oschin Schmidt Telescope is operated by the California Institute of Technology and Palomar Observatory

merging scenario and the accretion scenario.
The merging scenario is proposed by Bekki (1998), which assumes a head-on collision between two orthogonal spiral galaxies. The accretion scenario is proposed by e.g., Reshetnikov & Sotnikova (1997) and assumes the accretion of gas from another galaxy by the host galaxy. Two galaxies are assumed to interact, yet no merging is needed: Tidal interactions can account for gas accretion without any merging event. This last scenario is most supported by observations
Not only the optical emission of NGC 5014 shows peculiar features. The galaxy is surrounded by H I gas with a large tail of gas toward the south (Noordermeer et al., 2005).

In this report we present new and deeper observations of the centre of LGG 334 that have been carried out in the optical with the MDM 2.4m Hiltner telescope and in H I with the Westerbork Synthesis Radio Telescope (WSRT).
The WSRT is chosen, because the 21-cm line of neutral hydrogen can be used to study the distribution and kinematics of hydrogen gas in galaxy groups. H I is an extended disk tracer in normal galaxies and high resolution H I observations can be used to search for evidence of galaxy interactions within groups. The optical observations in the R and B-band will determine whether there are faint optical counterparts which can not be seen at the DSS images.
The purpose of this research is to analyze the new observations and try to explain the origin of the intergalactic H I clouds. When optical emission is detected, we can identify a new group member in the form of a very faint or dwarf galaxy. When no optical emission will be detected, we can give constraints on the observable magnitude limits at which no emission is detected. In that case, the H I gas has to be explained with one of the scenarios as mentioned before, like HVCs, primordial gas or tidal debris.
The observations will also put more constraints on the polar ring galaxy NGC 5014, its formation and a possible link with the intergalactic H I gas.
In section 2 the observations and data reduction will be described. The results of the observations will be presented in section 3. In the discussion in section 4, the results will be compared with several scenarios. Section 5 will end with a summary, conclusion and acknowledgments.

2. Observations and Data Reduction

Observations have been carried out at several wavelengths. Optical observations in the R and B-band have been performed with the MDM 2.4 Hiltner Telescope. H I observations are carried out with the Westerbork Synthesis Radio Telescope (WSRT). These wavelengths were chosen to best address the question, whether there exist stars in the gas rich regions between galaxies in the center of group LGG 334, and to provide more information on the dynamics of the gas clouds.

2.1. Radio Observations

The WSRT H I observations were carried out between February and June 2003. The central part of LGG 334 was observed four times for 12 hours. The first three times on February 15, February 25 and April 11. The fourth 12 hour observation was carried out over two days, May 20 and June 5.
The system was tuned to a central frequency of 1420 Mhz, to a corresponding heliocentric velocity of 1025 km s^{-1}. A summary of the observational parameters is given in Table 1.
The raw UV data are inspected and calibrated using the MIRIAD (Sault et al., 1995) package. Bad data points are flagged interactively. After flagging, the UV data are Fourier transformed to the image plane, and antenna patterns are calculated.
In each channel, maps were constructed at three different resolutions and corresponding noise levels. The first maps were produced using all available UV data-points, which resulted in a data cube with a resolution of $\sim$ 15 arcsec and a sensitivity of 0.28 mJy. The other two data cubes are produced, by down-weighting long baselines from the UV data. This resulted in spatial resolutions of respectively $\sim$ 30 and $\sim$ 60 arcsec and sensitivities of 0.4 mJy and 0.6 mJy per beam at medium and low resolutions. The synthesized beams of the three data cubes are respectively 23.26"$\times$14.25", 39.15"$\times$24.03" and 77.2"$\times$70.9" at full, medium and low resolution, at a channel spacing of 4.2 km s^{-1}.
When producing the images we used a value of 0 for the robust weighting parameter, R (Briggs, 1995). This robustness parameter can have various values to emphasize either the inner ($R > 0$) or outer ($R < 0$) regions of the UV plane (i.e., either large or small spatial scales). In practical terms, a higher R gives a higher spatial resolution at the expense of surface brightness sensitivity. $R = 0$ appeared optimal for our purpose.
The continuum has been subtracted by making a linear fit to the visibility data in a range of line free channels in either side of the band.
The four 12 hour observations were combined and images were made by CLEANing (Schwarz, 1978) the channels which showed line emission. A cleaning mask is used, to define the search areas.

Further data reduction has been performed by using the GIPSY package (Groningen Image Processing System; van der Hulst et al. (1992), Vogelaar & Terlouw (2001)). After careful inspection, the data cubes were integrated over the velocity axis to produce the zeroth and first order moment maps. In order to suppress the effects of noise, only data above a fixed threshold are used in the moment

	Data Set		
Parameters	High Resolution	Medium Resolution	Low Resolution
Phase center(α) (J2000)		13.11.54	
Phase center(δ) (J2000)		36.27.13	
Central velocity (heliocentric km s^{-1})		1025	
Primary beam (FWHM) (arcmin)		75	
Bandwidth (MHz)		20	
Observing band		21 cm	
Central Frequency (Mhz)		1420.405752	
Number of channels	225	300	225
Channel separation (km s^{-1})		4.2	
Robust parameter		0	
Synthesized beam:			
Major axis × minor axis (FWHM) (arcsec)	23.26 × 14.25	39.15 × 24.03	77.2 × 70.9
Noise level (1 σ):			
Flux density (mJy beam^{-1})	0.28	0.4	0.6
Column density ($\times 10^{18}$ cm^{-2} beam^{-1} ch^{-1})	3.9	2	0.5
Brightness temperature (K beam^{-1})	0.51	0.26	0.07

Table 1. Observational Parameters of H I

summation using the GIPSY task OBJECTS. This task applies a user specified threshold to a smoothed data cube and requires a user specified overlap between the emission of adjacent velocity channels. If a pixel in the smoothed data cube passes the threshold, the corresponding pixel in the original data is included in the moment analysis. A 4σ threshold is used for the OBJECT task and an overlap of at least 3 pixels is used with a depth of at least 3 channels. The output of this moment analysis is an integrated intensity map (zeroth-moment) and an intensity-weighted velocity map (first-moment).
The final zeroth-moment maps were corrected for primary-beam attenuation.

Although the high resolution data cube is of sufficient quality to derive useful H I maps and velocity fields, not all the emission is recognized. In the cases where the signal is very weak, the signal-to-noise ratio in the high resolution data cube is too low to extract the emission line profiles. In these cases the lower resolution data provide more useful information.
For the visualization of the data cubes the KARMA visualization package and the VIEW task of GIPSY have been used. These package were also used for the intercomparison of the radio and optical data. For creating figures, GPLOT was used.

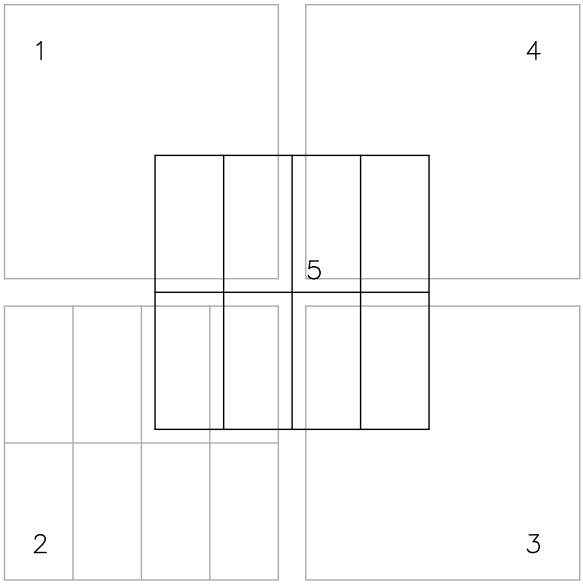

Fig. 1. The optical images are build up by five pointings. The central pointing is the fifth pointing, which overlaps the other four pointings, to get a deeper view. Each pointing is build up by eight chips, here this is shown for pointings 2 and 5.

2.2. Optical Observations

Optical observations have been carried out on 2002 December 30-31 and 2003 January 1 with the MDM 2.4m Hiltner Telescope.
Observations were carried out in the R and B-band. The R-band is used, because in this band, maximum sensitivity of the chip can be achieved. The B-band is the best band to look for low surface brightness galaxies and young stars.
The camera contains eight separate CCD-chips. Single images are created by combining these chips, these images are called pointings. Each single CCD-chip has 2044 × 4096 pixels, with a scale of 0".17 pixel^{-1}, resulting in a total field of view for one CCD-chip of 5.8' × 11.6' and 23.7' × 24.1' for one single pointing. The total field observed is build up by five pointings, as is shown in Fig. 1. During the optical observations, the conditions were photometric and the seeing was 2".7. The field of view of the total observed field is 49.2' × 51.7'.

Parameters	B-filter	R-filter
Date	2002 Dec 30/31	2003 Jan 01
Camera	MDM 2.4 m	MDM 2.4 m
Field of view:		
Single CCD frame	5.8' × 11.6'	5.8' × 11.6'
Single pointing	23.7' × 24.1'	23.7' × 24.1'
Total field	49.2' × 51.7'	49.2' × 51.7'
Center (RA)	13:12:49.89	13:11:46.00
Center (DEC)	36:39:48.52	36:27:57.72
Pixel size	0".17	0".17
Seeing	2".72	
Sky brightness (mag arcsec^{-2})		
1 σ surface brightness limit, unbinned (mag arcsec^{-2})	26.3	26.0
1 σ surface brightness limit, binning 5 × 5 (mag arcsec^{-2})	27.6	27.2
Effective exposure time (sec)	3600	2700

Table 2. Observational parameters of optical imaging

The first two nights all pointings have been observed four times during 900 seconds in the B-band. The third night, all pointings were observed three times for 900 seconds in the R-band. For each exposure the position of the telescope was shifted several arc-minutes to fill the gaps between individual chips and to minimize the effect of cosmetic defects on the CCD and cosmic rays.
The full data reduction has been performed by using the IRAF[2] package. Standard procedures of bias subtraction, flat-fielding and cosmic ray removal have been performed on the raw images. In IRAF the MSCRED package was used to handle the multi-extension files and combined images. All separate images were transferred to the same reference frame.
A rough coordinate system was created with the KOORDS task of the KARMA package. In the central pointing, the location of about 20 stars on each chip is referred to their coordinates on an image from the Digitized Sky Survey (DSS). A World Coordinate System (WCS) was fitted to all images using the tasks in the MSCRED package.
With the help of the WCS all chips are reprojected to the same reference point, which avoids position discrepancies especially at the outer edges of the image, when overlaying multiple images. The intensity scales of the single images were matched, cosmetic defects were removed and the single images were combined.
The photometric calibration of the data was done via the observations of standard Landolt stars; Landolt (1992). The photometry of the standard stars has been carried out using the DAOPHOT task in IRAF.

There is not much difference between the two images, although the B-band image is a little bit deeper because of the longer integration time. For the B-band image, the 1σ surface brightness limit is 26.3 mag arcsec^{-2}, while the R-band image has a 1σ surface brightness limit of 26.0 mag arcsec^{-2}. By binning the B-band image (which is the best band to look for young stars) 5 × 5 pixels, a surface-brightness limit can be achieved, of 27.63 mag arcsec^{-2}. This is more than 100 times dimmer than the central surface brightness of the disks of typical spiral galaxies (Freeman, 1970) and dimmer than any known massive low surface brightness galaxy (Bothun et al., 1987) or than the lowest surface brightness dwarf galaxy known (Zucker et al., 2004).
The R-band image has a 1σ surface brightness limit of 27.2 mag arcsec^{-2} when binning 5 × 5 pixels.

[2] IRAF is distributed by National Optical Astronomy Observatories, which is operated by the Association of Iniversitites INC. (AURA) under cooperative agreement with the National Science Foundation, U.S.A.

2.2.1. Ghost Images

In the optical images faint rings can be seen, especially around very bright stars. These faint rings might be ghost images. Ghost images are a common, but not widely noted, phenomenon in imaging with optical telescopes and CCD photometry. They have been investigated in detail for the Schmidt telescope by Yang et al. (2002).
Ghost images arise from multiple reflections in the telescope. Ghost images are much fainter than the primary image, therefore only the brightest stars produce ghost images.
In the MDM 2.4 m Hiltner observations, the ghost images have a ringlike circular shape. Their position is a little bit shifted from the position of the primary image, sometimes even overlapping it.

3. Results

3.1. Optical Images

Images of LGG 334, with a field of view of 0.82 × 0.86 degrees were created in the R and B-band. The B-band image is a little bit deeper than the R-band image.
In both images the four central group members can

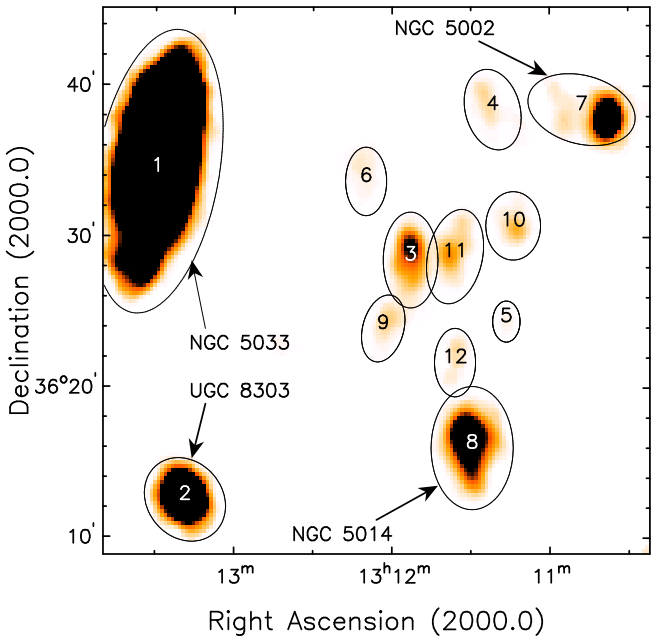

Fig. 2. Zeroth-moment map of the low resolution cube. The detected clouds are encircled and numbered from 1 to 12. If the cloud corresponds to a galaxy, this is mentioned in the figure. Eight clouds do not correspond to a galaxy.

be recognized with more detail than previous DSS observations, providing more information. Beside these four galaxies, no other galaxies or regions of faint optical emission can be seen. In the B-band image younger stars are expected, but there is no indication for star forming regions or blue dwarf galaxies to a surface brightness limit of 27.6 mag arcsec^{-2}, which is an important result. In the central area, which is the area of interest, all pointings overlap and the highest sensitivity is reached. Unfortunately in the outher parts of the images gaps can be seen on some places between pointings because they do not overlap. This does not hamper our study.

3.2. H I

All three cubes show a complex H I structure, with many separate complexes without obvious inter-connections. Even when the low resolution cube is smoothed, there are no signs of faint tails or bridges connecting the separate sources. In total twelve complexes are found. Some of them show a wealth of sub structure, and might consist of several subclouds. For describing them it is easier to assign them a number; (LGG334HI 1 - LGG334HI 12). If the origin of the source is clear, that means if the gas is from a group member, the name of the galaxy is used. LGG334HI 1, 2, 7 and 8 correspond respectively to the galaxies NGC 5033, UGC 8303, NGC 5002 and NGC 5014.
Figure 2 shows the twelve complexes in the zeroth moment map of the low resolution cube, their exact position is given in Table 4.

In Fig. 3 till Fig. 5, 36 channel maps are displayed of the central part of the medium resolution cube. Starting at 930 km s^{-1}, every second channel is plotted, so the difference in velocity between two channel maps is 8.4 km s^{-1}.
In the channel maps, only the inner, most interesting region of the group is displayed. The emission of NGC 5033 and UGC 8303 falls outside the plotted region. At the velocity of 930 km s^{-1}, the first H I complex appears, labelled LGG334HI 3. This complex vanishes at 997 km s^{-1}. At this velocity, in the upper right of the panel NGC 5002 appears. The velocity width of this galaxy and the plume of gas at the left is large, and the galaxy totally disappears at about 1148 km s^{-1}. The complex at the left of this galaxy, LGG334HI 4 is visible between 955 km s^{-1} and 997 km s^{-1}. In the channels where NGC 5002 appears in the top right, several other interesting features can be seen. At 1030 km s^{-1} the first emission of NGC 5014 appears. First only a kind of vertical plume can be seen, and the shape of the galaxy can not be recognized. At higher velocities, there is a lot of structure corresponding to a large tail at the south of the galaxy and the polar ring can be seen. The galaxy remains visible till the last panel shown, at a velocity of 1224 km s^{-1}.
At 1047 km s^{-1}, almost in the center of the panel, LGG334HI 9 appears, a complex at the south-east of LGG334HI 3. At 1081 km s^{-1}, LGG334HI 10 can be seen, which remains visible till about 1115 km s^{-1}. LGG334HI 11 is one of the largest intergalactic clouds observed here, which is visible between 1156 and 1207 km s^{-1}. Between LGG334HI 11 and NGC 5014, some emission can be seen at the same velocity of 1207 km s^{-1}, which remains visible in the following two pannels. This emission is caused by LGG334HI 12, which is almost connected to NGC 5014.

Figure 6 shows the B-band optical image, overlayed with column density contours derived from the medium resolution cube. Only the center of the group, where the intergalactic complexes appear is shown. In the image only the galaxies NGC 5014 and NGC 5002 can be seen. All intergalactic complexes do not have optical counterparts, down to our surface brightness level of 27.6 B mag arcsec^{-2} and 27.2 R mag arcsec^{-2}. In the complexes without an optical counterpart, the highest observed column density is about 6×10^{20} cm^{-2} in LGG334HI 3. Some complexes, like LGG334HI 4 and 10 have more than one component in this figure, although they are classified as one complex. This is because in the low resolution cube the components are connected. Most complexes do not look like dynamically bound sources, but have irregular asymmetric shapes. The H I distribution around NGC 5014 is quite unusual, in that the shape of the H I distribution is not at all aligned with the optical galaxy. The H I emission is much more

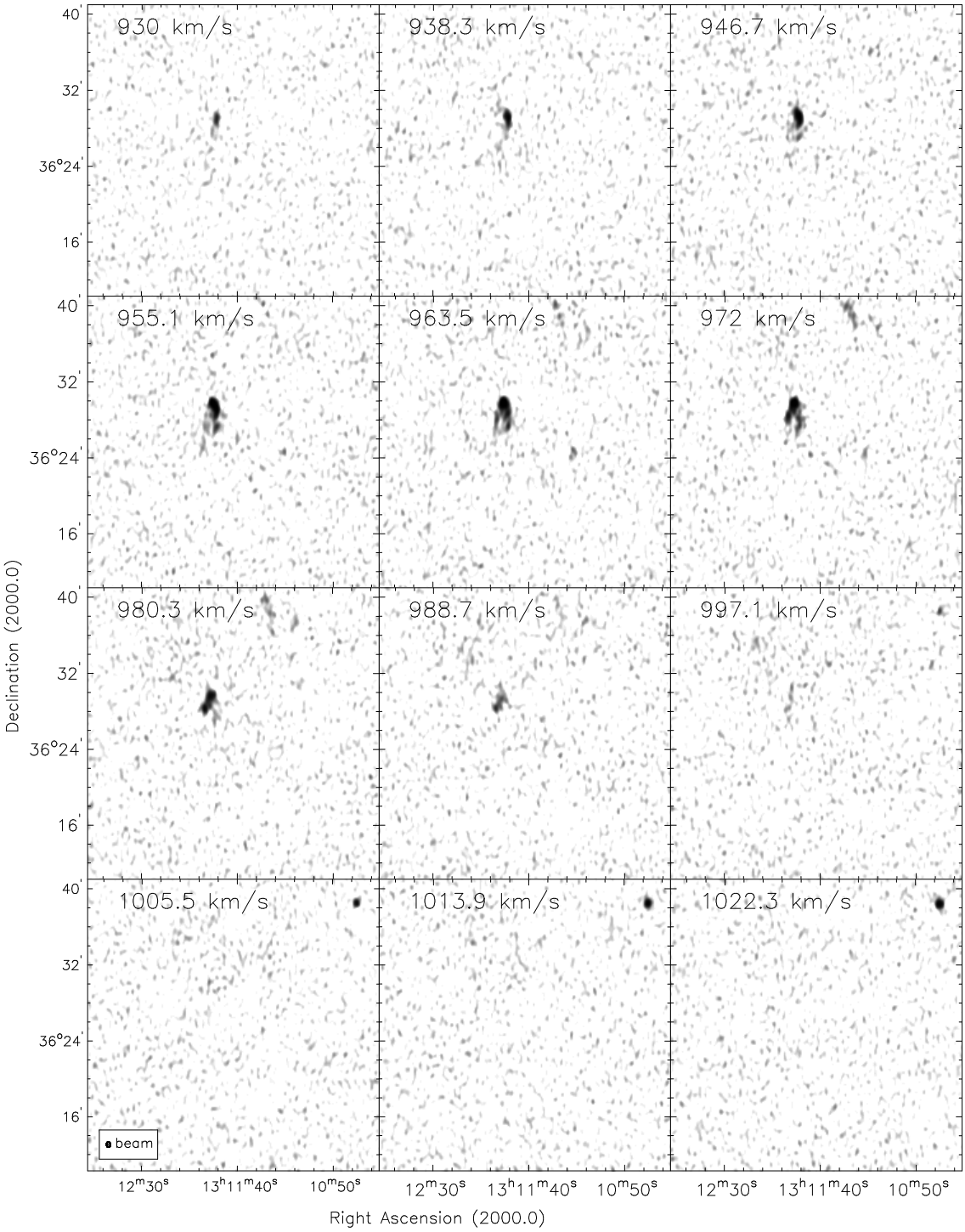

Fig. 3. H I channel maps of the central region of group LGG 334. The medium resolution cube is used, the beam size is indicated in the bottom left corner. In each panel, the heliocentric velocity is labeled. Starting at a velocity of 930 km s^{-1} every second channel is plotted till 1022.3 km s^{-1}

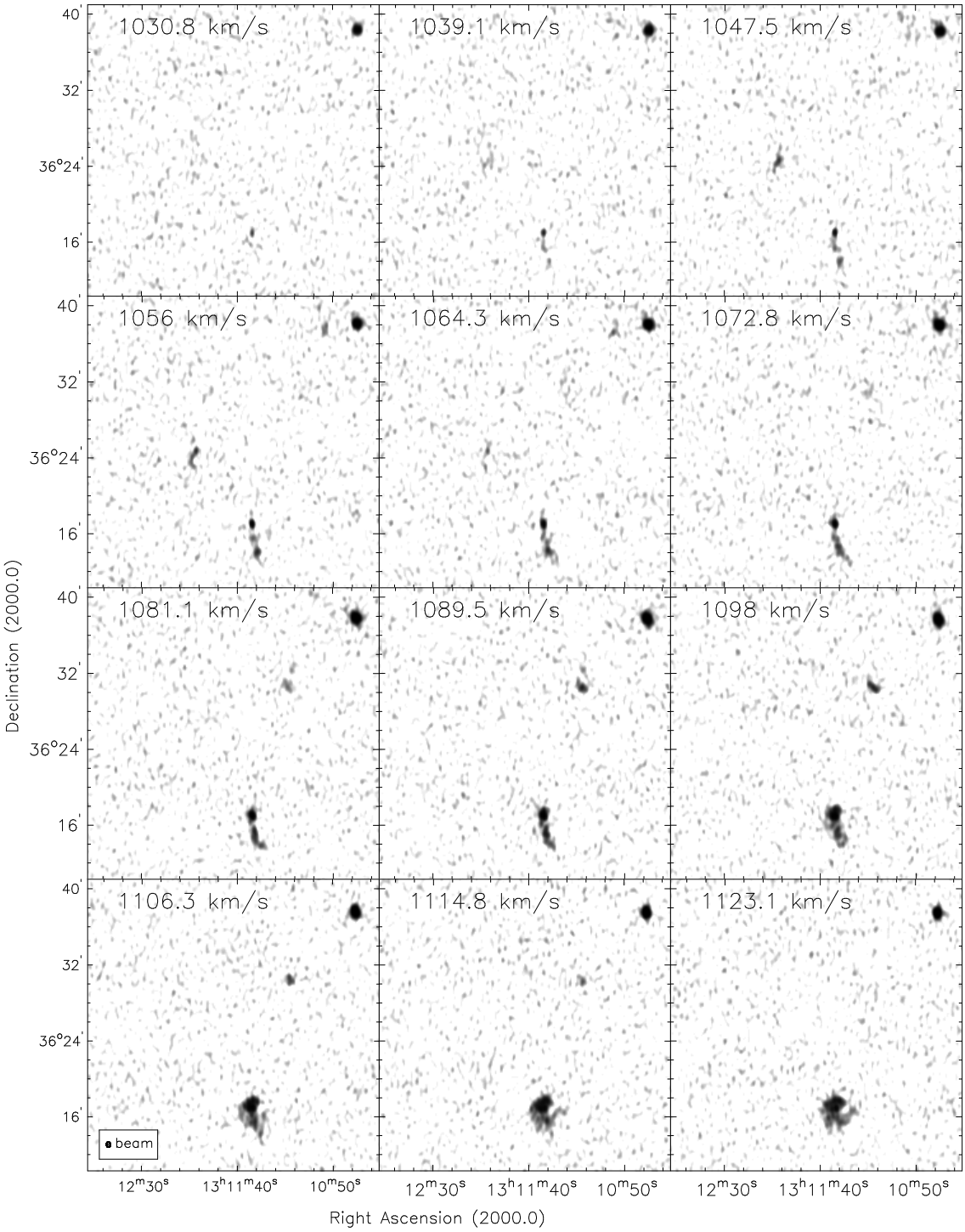

Fig. 4. H I channel maps of the central region of group LGG 334. The medium resolution cube is used, the beam size is indicated in the bottom left corner. In each panel, the heliocentric velocity is labeled. Starting at a velocity of 1030.8 km s^{-1} every second channel is plotted till 1123.1 km s^{-1}

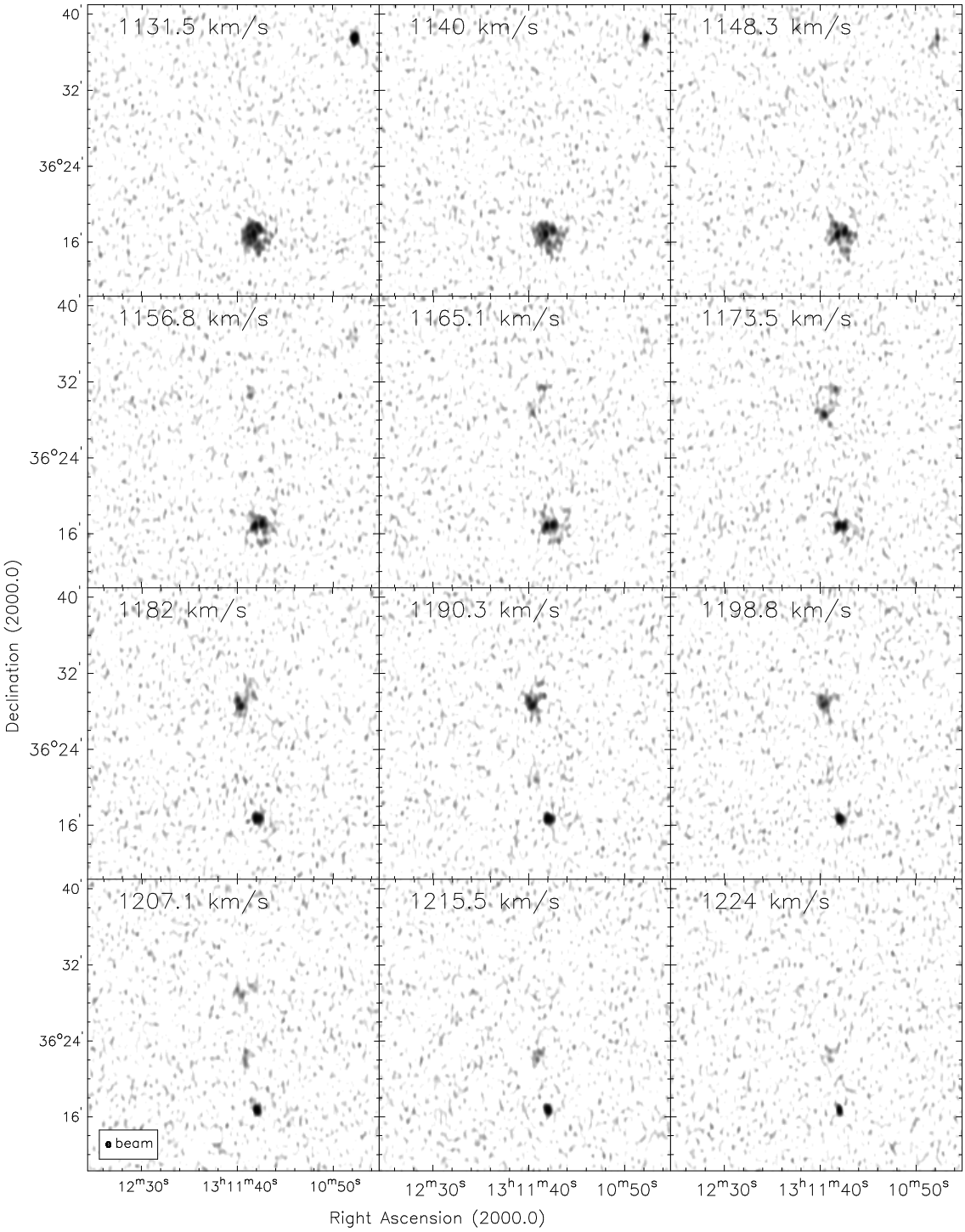

Fig. 5. H I channel maps of the central region of group LGG 334. The medium resolution cube is used, the beam size is indicated in the bottom left corner. In each panel, the heliocentric velocity is labeled. Starting at a velocity of 1131.5 km s^{-1} every second channel is plotted till 1224 km s^{-1}

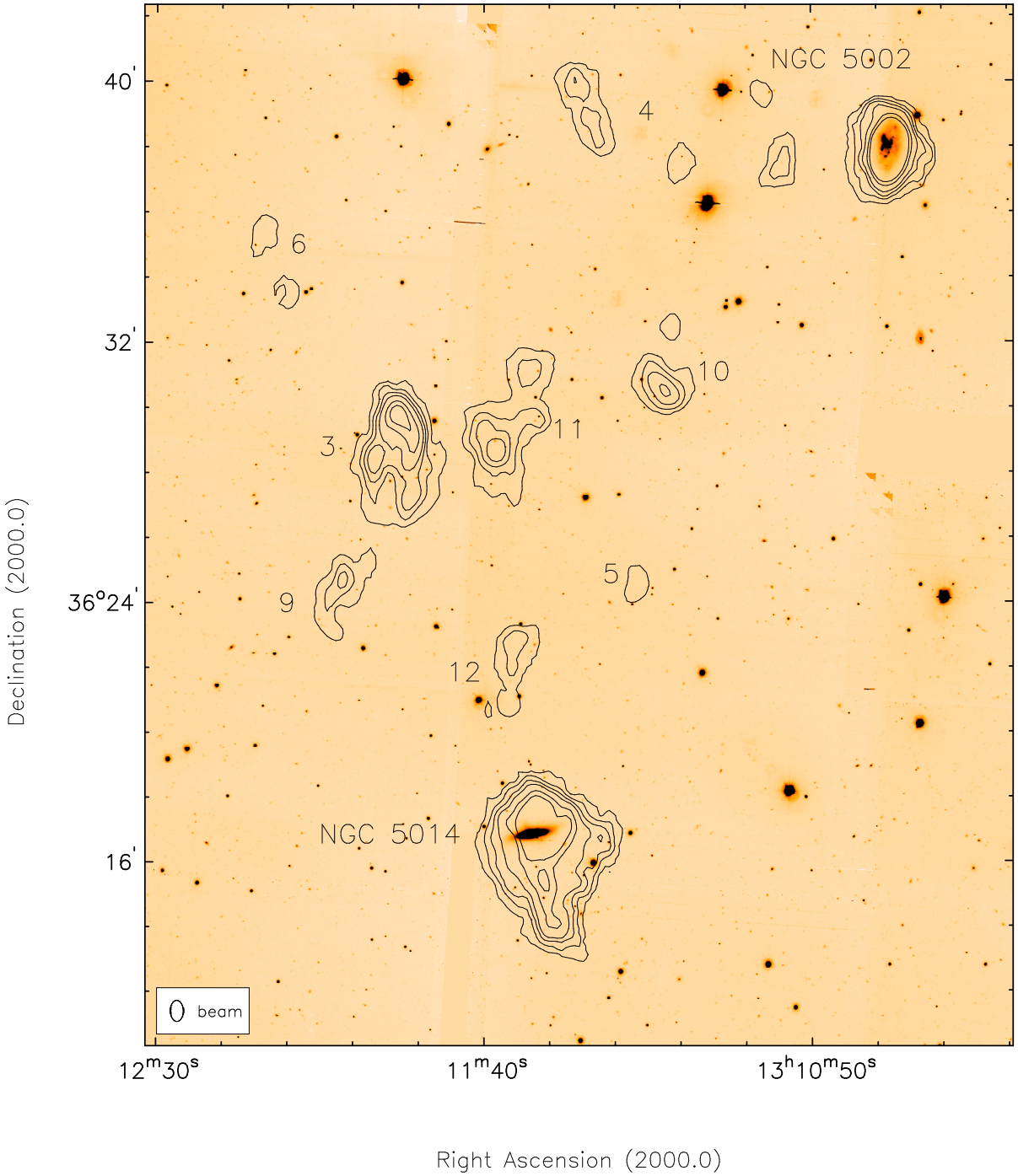

Fig. 6. *B*-band optical image with medium resolution contours of column densities at levels of $6 \cdot 10^{18}$, $3 \cdot 10^{19}$, $6 \cdot 10^{19}$, $1 \cdot 10^{20}$, $2 \cdot 10^{20}$ and $3 \cdot 10^{20}$ cm^{-2}. The size of the beam is 39" × 24", which is shown in the bottom left corner. For each H I complex the corresponding number is labeled.

extended and there is a large plume of H I gas. In the inner region, this plume has high column densities. No stars can be seen in this region.

Figure 7 shows the high resolution column density map, with contours of the medium resolution cube. Contours are drawn at the same levels as in the previous figure and the same region is displayed. Most complexes have very irregular asymmetric structures, especially LGG334HI 3 and LGG334HI 11. As mentioned before, very often they do not have a dense core, but are build up of several connected dense regions. Therefore they are probably not in dynamical equilibrium. Some complexes look like filaments, strings of small clouds, connected by diffuse streams. The complexes are more extended in the medium resolution cube and some emission structures cannot be seen in the high resolution map, like LGG334HI 6. In the low resolution cube the H I structures are even more extended, but no new complexes appear. There are no complexes that are clearly connected in the low resolution cube. The structure of the separate complexes will be discussed later.

Figure 8 shows the high resolution velocity map with velocity contours. The structure of the inner region of the group is complex. Separate complexes usually have very different velocities. NGC 5002 seems to rotate regularly. NGC 5014 is more complex. The inner part is rotating, but this rotational part is probably the polar ring. The outer parts of the galaxy seem to be rotating in a different direction. The H I complexes have small velocity gradients. Some complexes have almost a similar velocity, like LGG334HI 11 and LGG334HI 12, but no clear overall pattern can be recognized.
It might be that some complexes are connected in some way, because they have about the same radial velocities or are close to each other, like for example LGG334HI 11 and 12 or LGG334HI 3 and 4.
In Fig. 9 the global profiles of all detected sources are plotted . The top panel shows the group members and the down panel the H I complexes. In the top panel, a dotted line is drawn at the central radial velocity of NGC 5005, according to LEDA. This group member cannot be seen in our observations. It is interesting to see that the radial velocity of the H I complexes is close to the small group members and not to NGC 5033.

3.3. Distance to the group

For the group distance (i.e., distance to the center of mass) one wants to include the most massive group members, which are NGC 5005 and NGC 5033 in the case of LGG 334. Because a mass weighted mean is preferred, the small group members will not influence this mean value. Comparing the flux of NGC 5033 with the other observed group members, the flux in NGC 5033 is a factor $\sim 10-25$ larger as can be seen in Table 4 or the global profiles.

Galaxy	LEDA Rad.Vel. (km s^{-1})	WSRT Rad.Vel. (km s^{-1})
NGC 5002	1075	1072
NGC 5005	947	
NGC 5014	1132	1119
NGC 5033	878	873
UGC 8303	946	949

Table 3. Radial velocities of the central group members of LGG 334 in km s^{-1}. The second column shows the radial velocities received from the LEDA database and the third column shows the radial velocities determined by our WSRT observations. NGC 5005 is not observed, so no radial velocity is determined.

Although NGC 5005 has not been observed, this galaxy has a optical size comparable to NGC 5033 and cannot be neglected. The observed radial velocities are compared with the radial velocities from the HyperLeda[3] database in Table 3.
There is not much difference between these values, so for the radial velocity of NGC 5005, the velocity will be assumed as given by HyperLeda, without any correction. The average radial velocity of NGC 5005 and NGC 5033 is 910 km s^{-1}. This velocity has to be corrected for the Local Group infall onto Virgo. According to the HyperLeda database, the average correction for these galaxies is 202 km s^{-1} so this value is added, which gives a radial velocity of 1112 km s^{-1}.

Now the distance can be calculated with:

$$D = v/H \quad (1)$$

Where H is the Hubble constant for which 71 km s^{-1} Mpc^{-1} is used, v is the velocity (in km s^{-1}) and D is the calculated distance (in Mpc). This results in a distance to LGG 334 of 15.7 Mpc.

3.4. Properties of the gas complexes

The low resolution cube gives the best result for the total H I mass and flux of the gas complexes. In this cube also very faint extended emission can be recognized, which can not be seen in the high resolution cube. There seem to exist individual complexes at the same position but at different velocities, like LGG334HI 3 and LGG334HI 11. This causes an overlap of some sources in the zeroth moment map, therefore small cubes are made of the separate sources. With these small cubes of the individual complexes, properties can be determined, such as the integrated flux and the H I mass. The results are shown in Table 4.

[3] http://leda.univ-lyon1.fr/

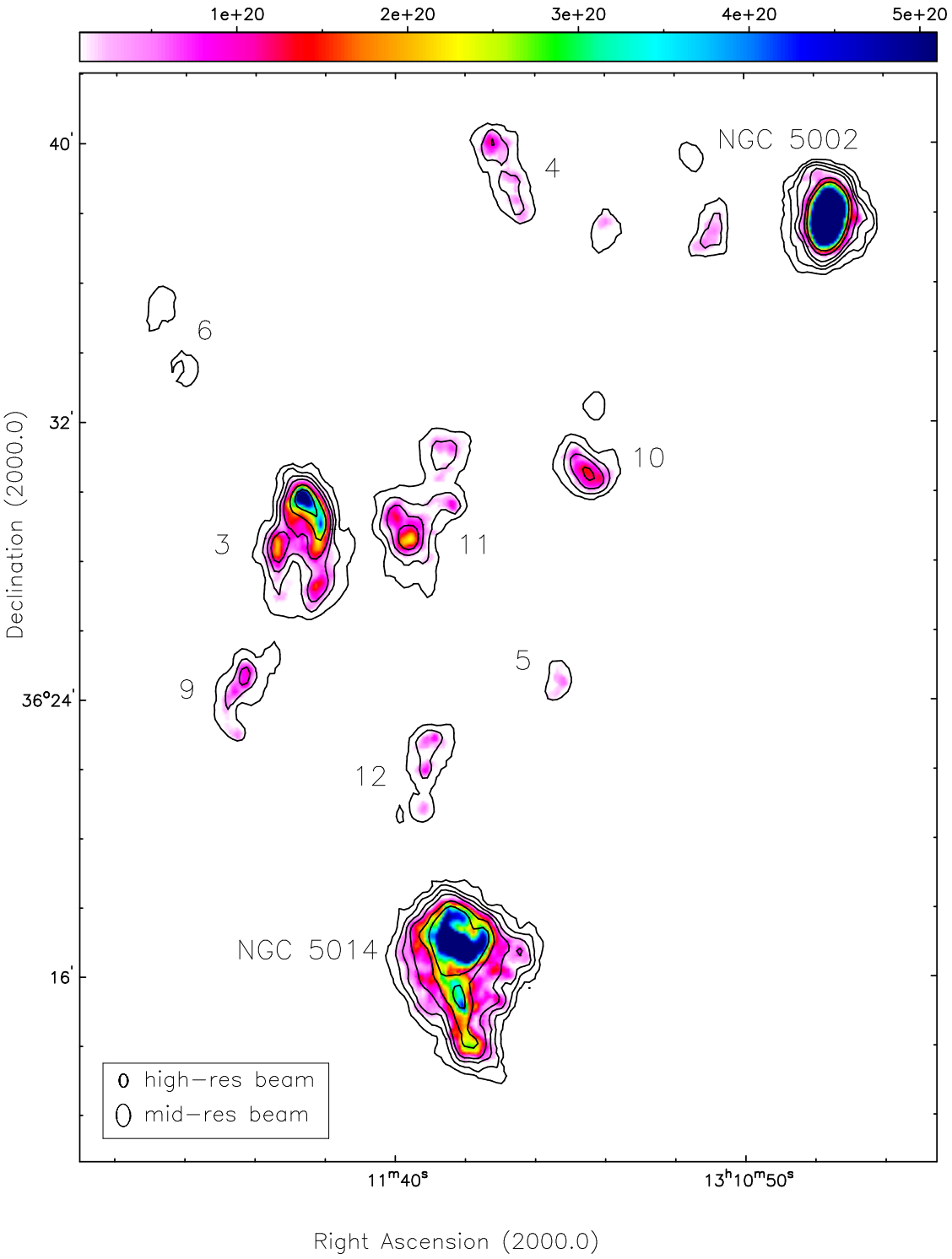

Fig. 7. Column density map of the inner region of the high resolution cube. On this map contours are drawn of the medium resolution column density map at levels of $6 \cdot 10^{18}$, $3 \cdot 10^{19}$, $6 \cdot 10^{19}$, $1 \cdot 10^{20}$, $2 \cdot 10^{20}$ and $3 \cdot 10^{20}$ cm^{-2}. The value of the colours are indicated by the colour bar in cm^{-2}.

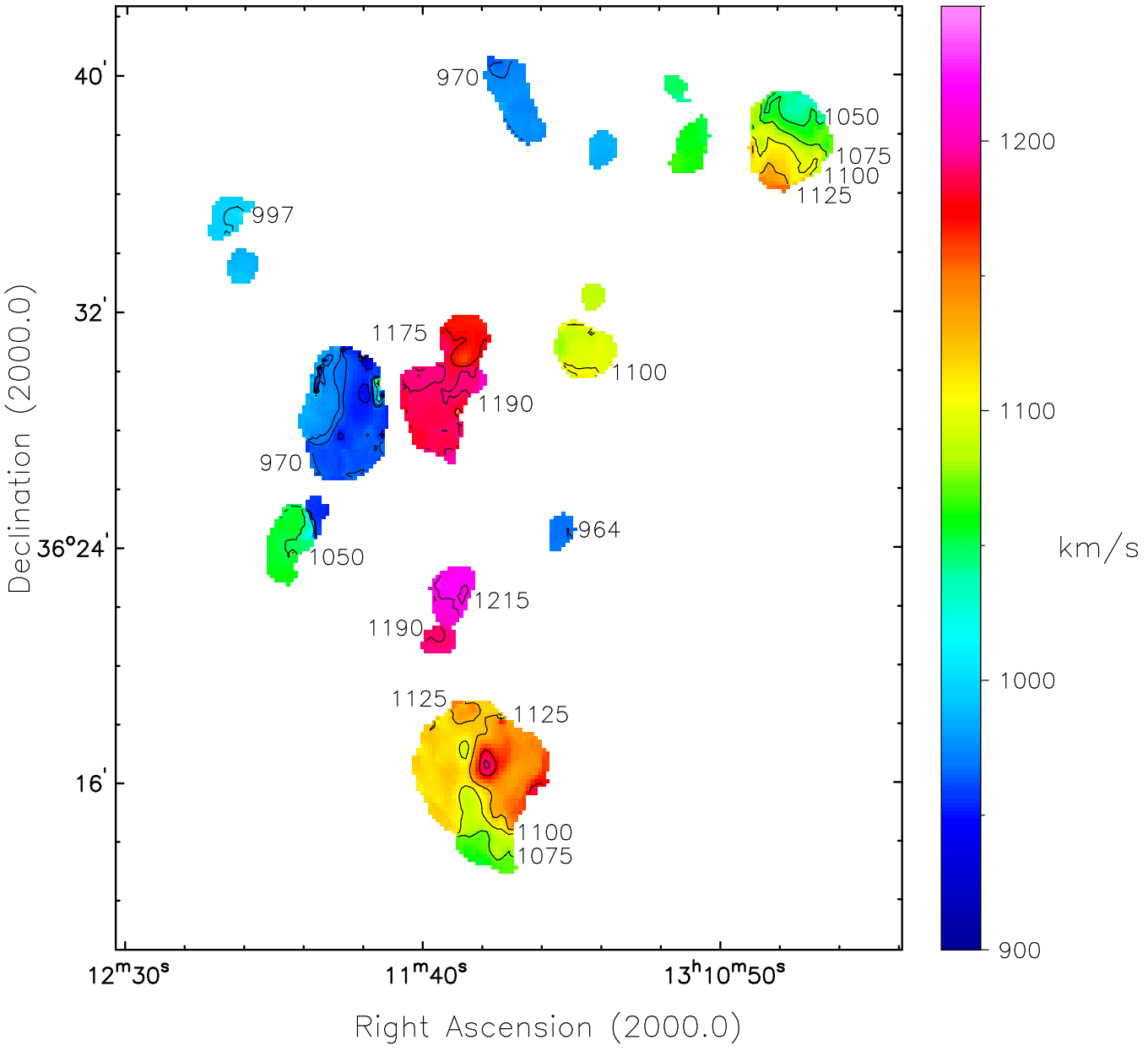

Fig. 8. High resolution velocity field of the inner region of group LGG334. The values of the colours are indicated by the colour bar. Velocity contours are drawn at the labelled velocities in km s^{-1}.

The total flux can be calculated by integrating over the global profile:

$$F = \sum S_{HI} \times dV \quad (2)$$

where S_{HI} is the line flux in each channel (in Jy) and dV is the channel spacing, which in this case is 4.2 km s^{-1}. With the integrated flux, the H I mass can be calculated, which is given by:

$$\frac{M_{HI}}{M_{\odot}} = 2.36 \cdot 10^5 \times D^2 \times F \quad (3)$$

where D is the distance to the group in (Mpc) and F is the integrated flux in (Jy). The H I mass is calculated (in $M_{\odot}$).

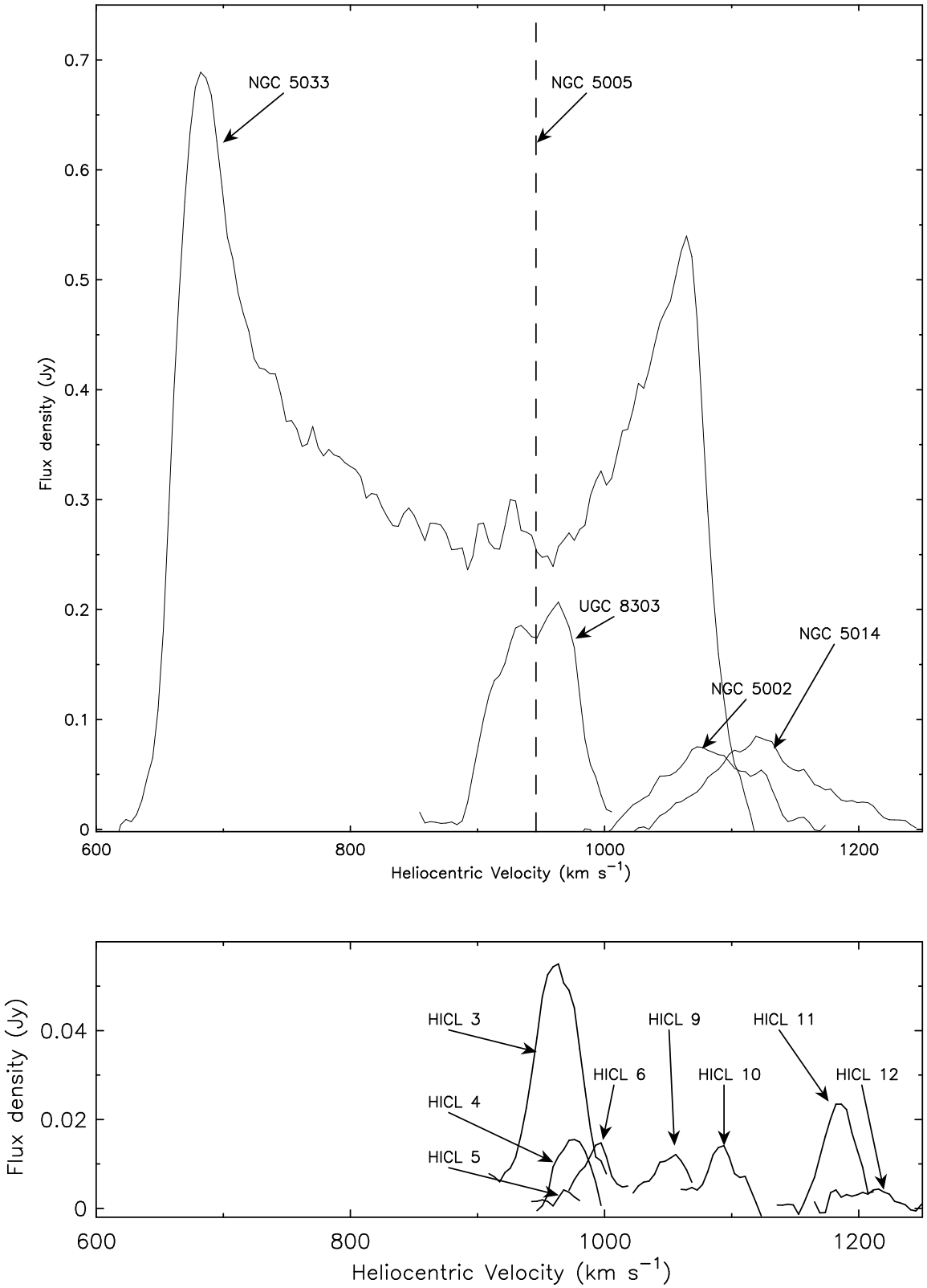

Fig. 9. Global profiles of the 12 H I emission sources. The top panel shows the four observed and classified group members and the bottom panel the 8 clouds without optical counterparts. Both panels have the same velocity scale, but the scale of the flux density is different, because in the group members the emission is much stronger. The dotted line in the top panel represents the radial velocity of NGC 5005 according to HyperLeda.

HI source	RA (J2000) h:m:s	DEC (J2000) ±d:m:s	Flux (Jy)	H I Mass ($M_\odot$)	ΔV (W20) (km s^{-1})	D (kpc)
NGC 5033	13:13:30	36:35:50	40.54	1.00×10^{10}	464	69
UGC 8303	13:13:19	36:12:53	3.43	8.4×10^{8}	101	15
LGG334HI 3	13:11:53	36:29:05	0.52	1.28×10^{8}	66	19
LGG334HI 4	13:11:24	36:38:40	0.07	1.59×10^{7}	40	22
LGG334HI 5	13:11:16	36:24:32	0.006	1.44×10^{6}	22	6
LGG334HI 6	13:12:12	36:34:40	0.038	0.94×10^{7}	50	22
NGC 5002	13:10:37	36:37:50	1.48	3.67×10^{8}	125	12
NGC 5014	13:11:30	36:16:46	1.97	4.86×10^{8}	164	14
LGG334HI 9	13:11:59	36:24:32	0.05	1.23×10^{7}	52	14
LGG334HI 10	13:11:13	36:30:56	0.084	2.07×10^{7}	52	11
LGG334HI 11	13:11:37	36:28:49	0.186	4.6×10^{7}	44	24
LGG334HI 12	13:11:36	36:22:24	0.04	0.97×10^{7}	61	16

Table 4. Global properties of the group members and H I complexes in the central part of LGG 334.

The brightness temperature is given by:

$$T_b = \frac{605.7383}{b_x b_y} \left(\frac{\nu_0}{\nu}\right)^2 \times S \quad (4)$$

T_b is the brightness temperature in Kelvin and b_x and b_y are the half power beam widths (HPBW) in arcsec. S is the line flux (in mJy). ν_0 is the rest frequency of the 21 cm line, which is 1.420405752 GHz.
The column density can be calculated from the brightness temperature:

$$N_{HI} = 1.823 \cdot 10^{18} \times \sum T_b \times dV \quad (5)$$

N_{HI} is the column density (in cm^{-2}), T_b is the brightness temperature in each channel and dV is again the channel spacing.
All H I properties of the sources are summarized in Table 4. The first three columns give the sources with their positions. In the fourth and fifth column the flux and mass are given. The sixth column gives the velocity width of the source, W20, which is the 21-cm line width at 20 percent of the peak of the profile (in km s^{-1}). These values are determined from the global profiles. In the last column the size (D) of the sources is given. For the group members, the diameters are derived at a surface density of 1 M$_\odot$ pc^{-2}. This is not possible for the other complexes, because of the filamentary structure with more dense components. For these sources an estimate of the length is given.

3.5. The Separate Complexes

For each H I emission source, small cubes have been made, to isolate them. For each complex or group member, we summarize the properties below.

3.5.1. NGC 5033:

NGC 5033 is a Seyfert galaxy, classified as SA(s)c. The H I mass of this galaxy is $1.00 \times 10^{10} M_\odot$, with an H I diameter of about 69 kpc. Figure 10 shows several representations of the galaxy. In the left panel the optical B-band image is plotted. In the optical clear spiral arms can be seen, the optical diameter is about 47 kpc. This image is overlayed with contours of the medium resolution column density map. The contour levels are indicated in the figure; the high column densities are not shown in this panel.
The second panel shows the high resolution column density map, which shows much structure. The inner regions of the galaxy have column densities up to 2.8×10^{21} cm^{-2}. Spiral arms can be seen, but extending from the southern part of the galaxy is an asymmetric plume of gas with a size of 13 kpc. As can be seen in the first panel, this plume does not seem to have an optical counterpart. However, unfortunately this galaxy is at the edge of the mosaic, so there is a gap at the corresponding position in the optical image. Therefore we cannot be sure whether there is no optical counterpart.
The right panel shows the first moment map. Velocity contours are shown, from 700 to 1050 km s^{-1}. The velocity field has the characteristics of regular rotation. The kinematics have been studied in detail by Thean et al. (1997), they claim to have found some evidence for a previous tidal encounter of the galaxy.

3.5.2. UGC 8303:

UGC 8303 is classified in the Nasa Extragalactic Database as an irregular dwarf galaxy IAB(s). The H I mass is $8.4 \times 10^8 M_\odot$. The upper left panel of Fig. 11 shows the B-band optical image, with H I contours from the medium resolution column density map. The core of this galaxy appears irregular; no clear structure can be recognized. In the outer parts however, faint spiral arms can be recognized, especially at the left side. The optical radius is about 7 kpc and the H I radius is 19 kpc. The optical emission is very asymmetric; there is diffuse emission in the down-right of the optical image, while at the left part, there is almost no emission. In the column density map in the middle panel it is also interesting to see that in H I

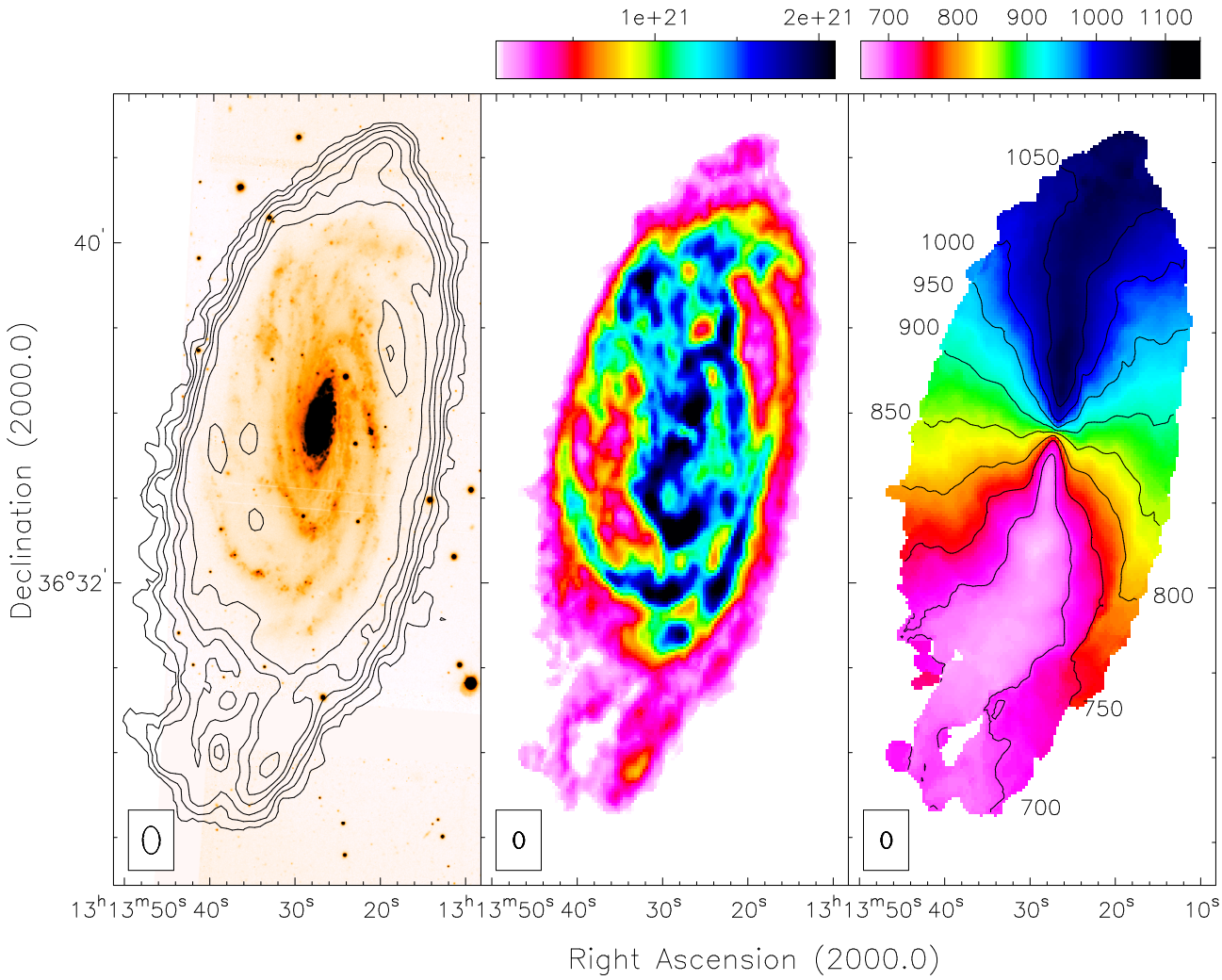

Fig. 10. Optical and H I images of NGC 5033. The left panel shows the B-band optical image. In this panel contours are drawn of the medium resolution column density map at levels of 1×10^{19}, 5×10^{19}, 1×10^{20}, 2×10^{20}, 3×10^{20} and 5×10^{20} cm^{-2}. The middle panel shows the high resolution column density map, the densities correspond to the colour bar in cm^{-2}. The right panel shows the high resolution velocity map, the velocities correspond to the colours in the colour bar. Contours are drawn at the labelled velocities in km s^{-1}. The medium resolution beam is plotted in the bottom left of the left panel, the high resolution beam is plotted in the bottom left of the other panels.

the center is not the densest part of the galaxy. Around the center a kind of ring can be recognized with more H I gas. Towards the left, where in the optical a spiral arm can be recognized, the column density is also somewhat higher. The column density goes up to $1.5{\times}10^{21}$ cm^{-2}. The velocity field in Fig. 11 is labelled between 905 and 975 km s^{-1} and has characteristics of regular rotation.

3.5.3. LGG334HI 3:

LGG334HI 3 is a large complex with a peculiar shape. Amongst the sources found, this is the largest source which is not linked to a known group member. In Fig. 12 the high resolution column density map is plotted. This image is overlayed with contours of the medium resolution column density map. With an H I mass of $1.28 \times 10^8 M_\odot$ it could have been a dwarf galaxy; e.g., Swaters et al. (2002). There is however no optical counterpart neither in the B nor in the R-band image. The size of the complex is about 19 kpc with a maximum column density of $6{\times}10^{20}$ cm^{-2} in the inner part. The structure is very asymmetric and has a little bit the shape of a horse shoe. The northern part of the cloud is the part with the highest density. This high density arc has two fainter tails, ending in blobs with again a little bit higher density. On the column density map, especially at low resolution, it seems that this cloud is connected with two other clouds, LGG334HI 9 and LGG334HI 11. In Fig. 9 these clouds can be seen at

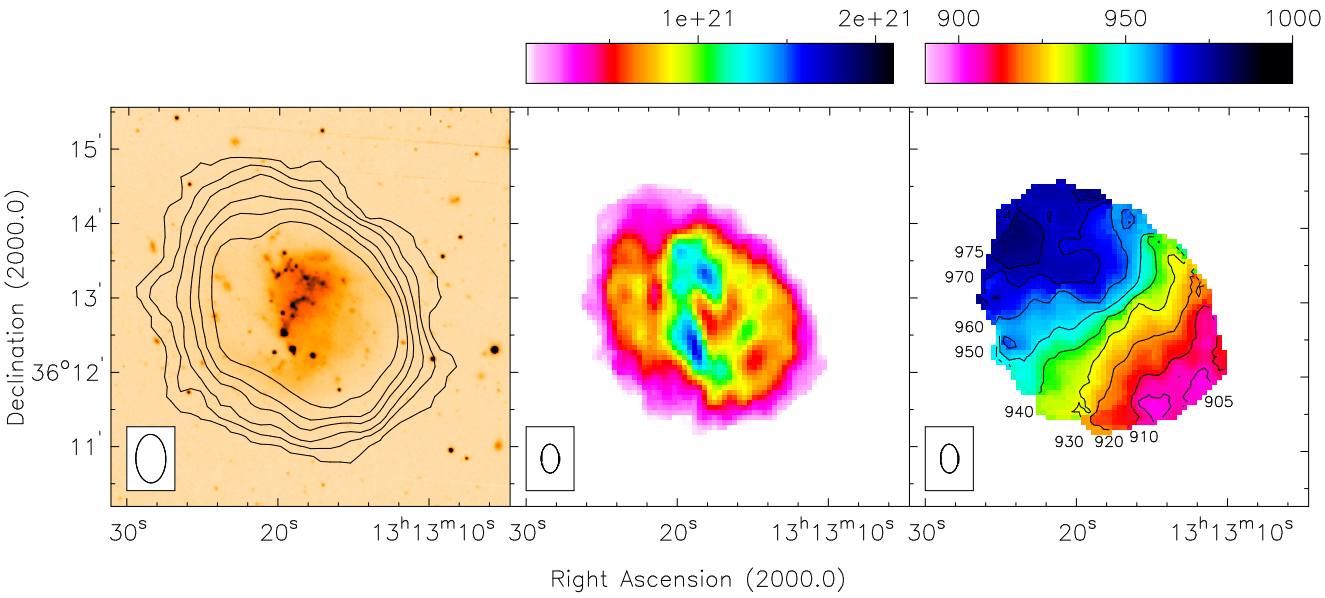

Fig. 11. Optical and H I images of UGC 8303. The left panel shows the B-band optical image. Contours are drawn of the medium resolution column density map at levels of 1×10^{19}, 5×10^{19}, 1×10^{20}, 2×10^{20}, 3×10^{20} and 5×10^{20} cm^{-2}. In the bottom left, the medium resolution beam is plotted. The middle panel shows the high resolution column density map and the right panel the high resolution velocity map; in both panels the high resolution beam is plotted.

different velocities, so they are separated entities.
When a x, v slice is taken of LGG334HI 3 through the data cube along a spline, no more information can be obtained. All the dense parts are physically connected and the peculiar shape is probably caused by the projection angle, suggesting that this complex is an elongated arc of H I gas, which is projected on the x, y plane.

3.5.4. LGG334HI 4:

The velocity width of this complex is 40 km s^{-1}, centered at 972 km s^{-1}. The H I mass of the cloud is $1.59 \times 10^7 M_\odot$ with a size of 22 kpc when all the dense parts are taken in. The cloud does not have an optical counterpart.
In Fig. 13 the high resolution column density map is plotted with the contours of the medium resolution map overlayed. The maximum column density is about $1{\times}10^{20}$ cm^{-2}, however this is only a single spot, the main part is much fainter. No clear structure can be recognized in the H I. The inner region contains three knots from north to south with a high density with respect to the rest of the cloud. There is a small tail toward the right with a spot at the end, the column density here is about $3.5{\times}10^{19}$ cm^{-2}. In the low resolution map all four dense regions are connected. Although no bridge is seen, there might be a connection with NGC 5002. However, there is a difference in velocity of about 80 km s^{-1} between LGG334HI 4 and NGC 5002.

3.5.5. LGG334HI 5:

This complex is the smallest one found in the region. The velocity width is about 22 km s^{-1}, centered at 964 km s^{-1}. The mass of this cloud is $1.44 \times 10^6 M_\odot$ with a highest column density of $7{\times}10^{18}$ cm^{-2}. The size of the complex is about 6 kpc. In the center, there is a small denser part, with two small extensions toward the north and south, as can be seen in Fig. 7.

3.5.6. LGG334HI 6:

The highest column density of this complex in the low resolution map is $1{\times}10^{19}$ cm^{-2}, however the cloud is not visible in the high resolution map. LGG334HI 6 has a size of about 22 kpc and the mass is $0.94 \times 10^7 M_\odot$. The velocity range is 50 km s^{-1}, centered at 997 km s^{-1}. This cloud does not have a clear inner region, it contains two spots with a higher column density than the surroundings.

3.5.7. NGC 5002:

NGC 5002 is an irregular galaxy, classified in the Nasa Extragalactic Database as SBm. The H I mass of this galaxy is $3.67 \times 10^8 M_\odot$. In Fig. 14 the B-band optical image, the high resolution H I column density map and the high resolution velocity field are plotted. On the optical image, contours are drawn of the medium resolution column density map.
The shape of the H I of the galaxy seems symmetric,

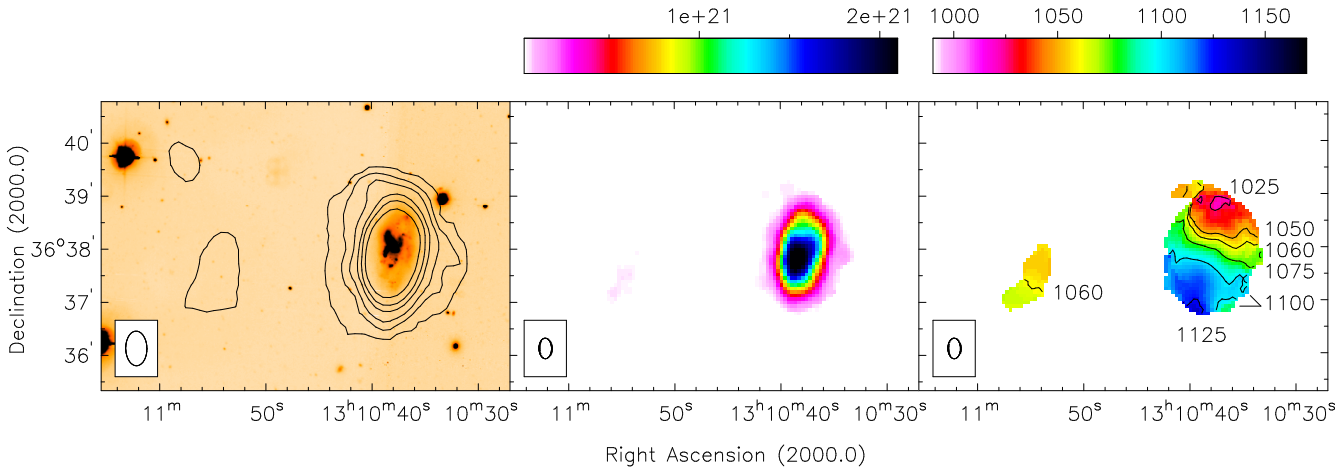

Fig. 14. Optical and H I images of NGC 5002. The left panel shows the *B*-band optical image. Contours are drawn of the medium resolution column density map at levels of 1×10^{19}, 5×10^{19}, 1×10^{20}, 2×10^{20}, 3×10^{20} and 3×10^{20} cm^{-2}. In the down left, the medium resolution beam is plotted. The H I sources left from the galaxy do not have an optical counterpart. The middle panel shows the high resolution column density map and the right panel the high resolution velocity map. Velocity contours are drawn at the labeled velocities. In the middle and left panel, the high resolution beam is plotted.

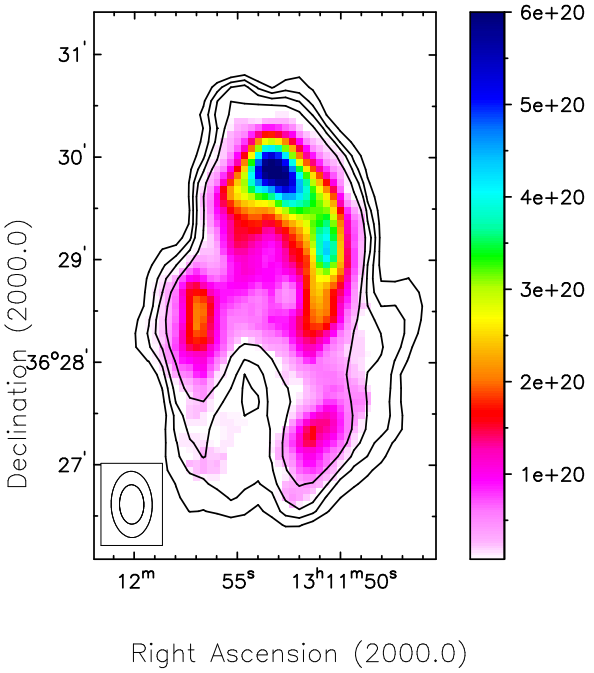

Fig. 12. High resolution column density map of LGG334HI 3. Contours are drawn of the medium resolution column density map at levels of 1×10^{19}, 2×10^{19}, 3×10^{19} and 5×10^{19} cm^{-2}. The colours correspond to the colour bar next to the image, in cm^{-2}. In the bottom-left corner, the high resolution beam is plotted within the medium resolution beam.

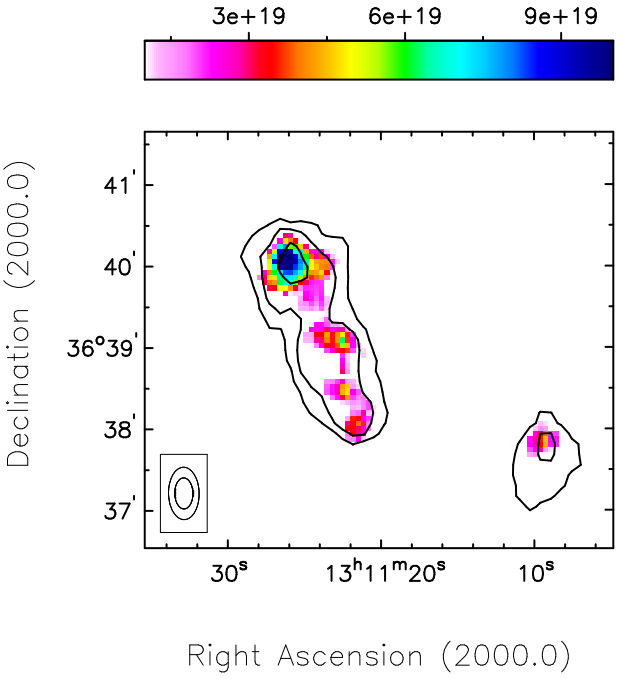

Fig. 13. High resolution column density map of LGG334HI 4. Contours are drawn of the medium resolution column density map at levels of 6×10^{18}, 2×10^{19} and 5×10^{19} cm^{-2}. The colours correspond to the colour bar above the image, in cm^{-2}. In the bottom-left corner, the high resolution beam is plotted within the medium resolution beam.

however on the left part, there is a kind of tail aimed to the north-west direction with a size of about 15 kpc towards LGG334HI 4. In the low resolution data, this tail is connected with the galaxy. LGG334HI 4 did have a small tail towards NGC 5002. The two tails are not connected, however this is an indication, that this galaxy and its neighbor cloud might be connected. The highest

column density found in the galaxy is 2.2×10^{21} cm^{-2}, the tail at the west parts has two knots with a higher density, compared to the rest of the plume. One of these knots cannot be seen in the high resolution map, however in the medium resolution map, both knots are visible. The column densities found in these regions are about 1×10^{19} cm^{-2}. Furthermore a small extension can be recognized in the top-left of the galaxy, but this is not connected with the other extended H I emission. Although this extension is very small, there is a difference in velocity.
The velocity field in the right panel shows clearly that the galaxy is rotating.

3.5.8. NGC 5014:

This galaxy is one of the most interesting objects in the group, because of its polar ring. In the Nasa Extragalactic Database, the galaxy is classified as a Sa spiral galaxy, however with a question mark. Because the galaxy is edge on, spiral structure is not easy to notice. In Fig. 15 one can see at first sight, that the H I structure of this galaxy is very complex. The left panel shows the B-band optical image. In addition to the main disk, there are two extensions on each side of the galaxy, which look like a polar ring. These extensions are tilted about 45 degrees from the main disk. The optical diameter of the main disk is about 7 kpc according to Leda. The diameter of the second disk, which looks like a polar ring, is much smaller.
The optical image is overlayed with the contours of the medium resolution column density map. Clearly the structure of the optical and of the H I are not the same. The H I emission is much more extended, and there is a very large tail of H I gas to the south of the galaxy. The middle panel of this figure shows the high resolution column density map. Again one can see, that the H I gas is highly extended. The densest regions are not aligned with the main disk of the galaxy, but with the polar ring. Also the tail towards the south is denser than the surrounding gas. The column density in the center goes up to 1.9×10^{21} cm^{-2}, while the column density in the tail reaches 4×10^{20} cm^{-2}.
The velocity field in the right panel of Fig. 15 is very complex. In the center, a rotational part can be recognized which is aligned with the polar ring. The velocity difference here is about 150 km s^{-1}. It seems that there is also some rotation which is horizontally aligned. However, it is hard to say whether this is the rotation of the main disk, or that it is extended gas from the polar ring. The large tail towards the south has the same velocity as the left part of the polar ring. The diameter of the galaxy in H I is about 14 kpc, while the length of the plume is about 15 kpc. The total H I mass in NGC 5014 is $4.86\times10^8 M_\odot$. The velocity range of the galaxy is about 164 km s^{-1}, centered at 1130 km s^{-1}.
Obviously NGC 5014 is a peculiar galaxy. Something has caused the large plume of gas and something has caused the polar ring. The galaxy seems connected with LGG334HI 12, this is shown in Fig. 16. In the top panel the line denotes the slice that is taken in the velocity plane of the low resolution cube. In the bottom panel three bright regions can be seen in the slice, the largest one is NGC 5014 at the right. Next to the galaxy a smaller source seems connected to the galaxy, this is LGG334HI 12. The source on the left is LGG334HI 11, this cloud is not connected to LGG334HI 12, but has almost the same velocity.

3.5.9. LGG334HI 9:

This cloud is in position very close to LGG334HI 3, however the first moment maps and the spectra in Fig. 9 show that these two clouds are at different velocities, indicating that the overlap in position is probably the result of a projection along the line of sight. This cloud does not have an optical counterpart, the H I size is about 14 kpc from north to south. When looking at the contours this galaxy has a little bit an arc shape. The total H I mass is $1.23\times10^7 M_\odot$ and the maximum column density is 7×10^{19} cm^{-2}. The velocity width is about 52 km s^{-1}, centered at 1047 km s^{-1}.

3.5.10. LGG334HI 10:

This looks like a spherical cloud, but at the north there is a small knot. This knot is physically connected with the cloud, it also has the same velocity. The velocity width of LGG334HI 10 is 52 km s^{-1}, centered at 1094 km s^{-1}; it does not seem to rotate. The knot cannot be seen in the high resolution map, but is visible in the medium and low resolution maps. The maximum column density is 1×10^{20} cm^{-2} and the mass is $2.07\times10^7 M_\odot$. This cloud also does not have an optical counterpart, the H I diameter is about 11 kpc.

3.5.11. LGG334HI 11:

At first sight it looks as if this cloud is connected with LGG334HI 3 because they look connected in the first moment maps. However these are two separate clouds which can be clearly seen in the first moment maps. This cloud is one of the biggest clouds, with an H I mass of $4.6\times10^7 M_\odot$, it does not have an optical counterpart. The cloud does not have a clear morphology, it contains a denser inner region with a column density up to 1.5×10^{20} cm^{-2}. It has a tail toward the north and a little bit to the west, containing two denser regions. The column densities in these two dense spots are about 4×10^{19} cm^{-2}. Again this source does not have any optical counterpart, but the H I size is 13 kpc and about 24 kpc when the tail is taken in. The velocity width of the cloud is 44 km s^{-1}, centered at 1174 km s^{-1}; it does not seem to rotate

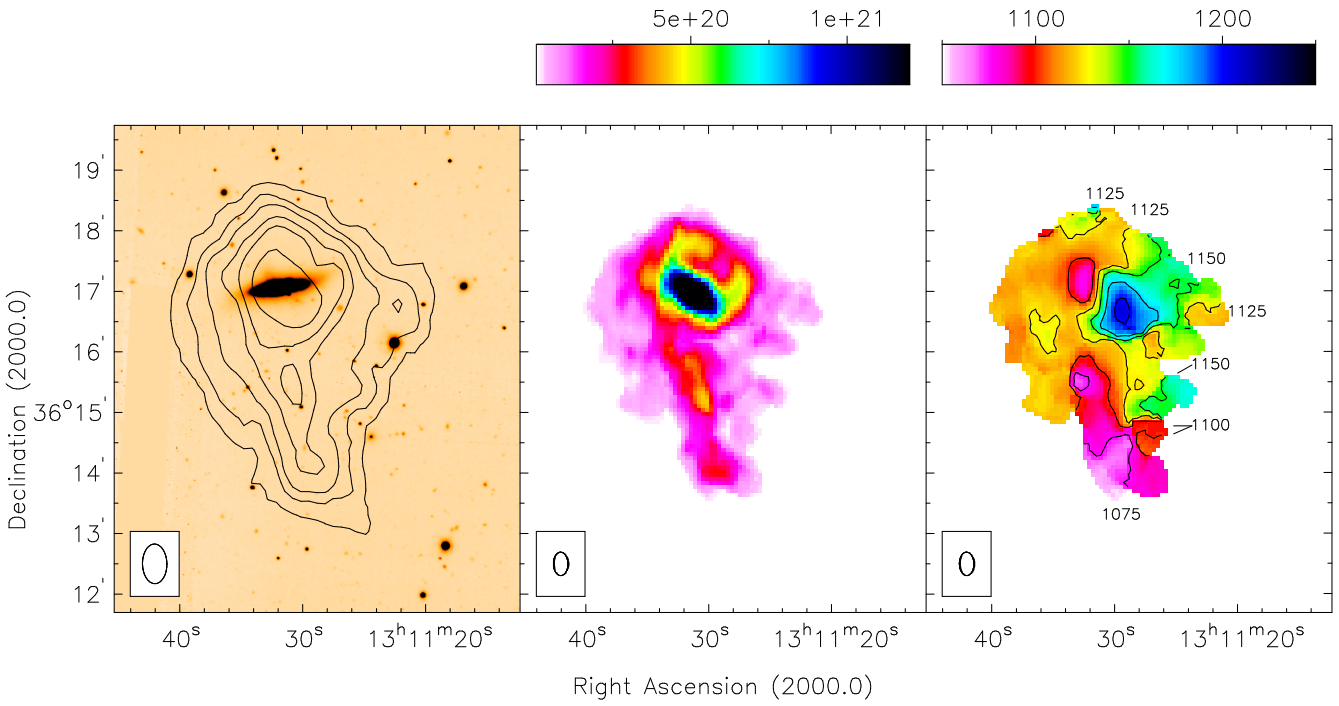

Fig. 15. Optical and H I images of NGC 5014. The up left panel shows the B-band optical image. Contours are drawn of the medium resolution column density map at levels of 1×10^{19}, 5×10^{19}, 1×10^{20}, 2×10^{20}, 3×10^{20} and 5×10^{20} cm^{-2}. A large plume of H I can be seen to the south, without an optical counterpart. The optical disk has two extensions. In the down left of the first panel, the medium resolution beam is plotted. The middle panel shows the high resolution column density map and the down left panel the high resolution velocity map, contours are plotted at the labelled velocities. In the middle and right panel, the high resolution beam is plotted.

3.5.12. LGG334HI 12:

Although this cloud is pretty small, it is very interesting. The cloud is located at the north of NGC 5014 and there are indications that it is physically connected to NGC 5014. This cloud therefore is probably related to the polar ring and/or the large plume of H I gas at the south of NGC 5014 as can be seen in Fig. 16. This cloud is actually not one cloud with one clear inner region, but it has three denser regions from north to south. The total H I mass is $0.97 \times 10^7 M_\odot$ and the column densities in two of the three knots goes up to about $6{\times}10^{19}$ cm^{-2}. LGG334HI 12 also does not have any optical counterpart, but in H I it is about 16 kpc long and the width is about 5 kpc. This cloud could form a bridge toward NGC 5014 and maybe LGG334HI 11. These two clouds are not physically connected, but the velocities are almost the same. The velocity width of LGG334HI 12 is about 61 km s^{-1}, centered at 1211 km s^{-1}.

3.6. Other H I sources

Two sources of H I emission are found just at the border of the data cubes. These sources are outside the optical images, so can not be seen. The first source is a small dwarf galaxy, UGC 8314, located at the north east of UGC 8303. This group member is not very interesting and will not be discussed further.

The second source is a small H I cloud, about 30 kpc east of NGC 5033. It is very likely that this is also a cloud without an optical counterpart, because at the location there is no known group member. This small H I cloud is mentioned before by Thean et al. (1997). No other H I sources are found in our observations at the west of NGC 5033. Unfortunately this H I cloud is far out the center of the H I observations, outside the primary beam and the measurements are not very sensitive. The determined properties of this single object are shown in Table 5.

Center (RA J2000)	13:14:20.46
Center (DEC J2000)	36:34:22.32
Flux (Jy km s^{-1})	0.097
HI Mass ($M_\odot$)	2.74×10^6
Velocity Range (km s^{-1})	1177 - 1202
R (kpc)	4.8

Table 5. H I properties of the single source west of NGC 5033.

4. Discussion

In the center of LGG 334, eight H I clouds do not have an optical counterpart. The structure of these clouds is very complex. Some of them have a filamentary structure

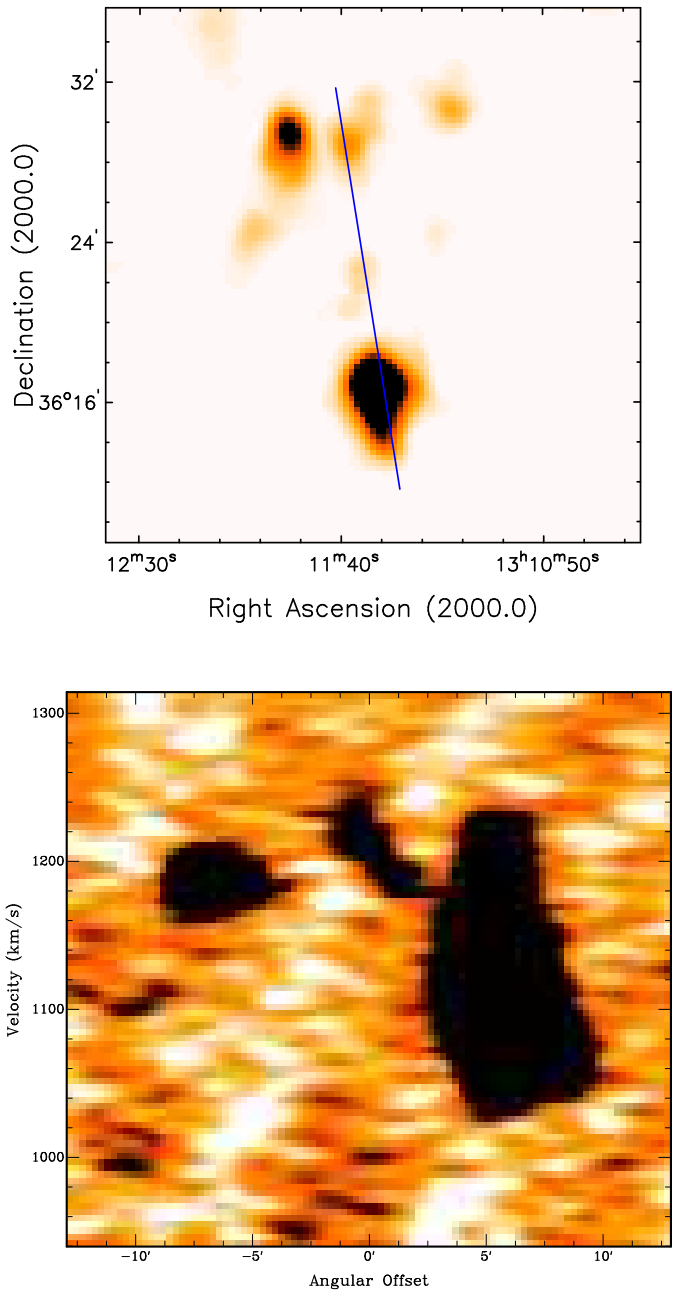

Fig. 16. Upper panel shows a part from the zero moment map of the low resolution cube. The blue line indicares the slice that is taken. The lower panel shows this slice in the RA-velocity plane.

and are build up of several smaller clouds, connected by a kind of bridge. None of the clouds is symmetric and even the more dense parts, or the sub-clouds do not seem to be spherically symmetric. Because of this complex structure, it is hard to put constraints on the volume density or the dynamical mass. For both, a spherical symmetric appearance needs to be assumed.
The results can be compared with some scenarios to try to put more constraints on the origin of the H I complexes.

It does not seem plausible that the observed H I complexes are primordial. As stated by Briggs (2005) intergalactic H I clouds are always in the neighborhood of galaxies. This is also the case for LGG 334. There is no hard proof for detected primordial matter in the form of H I clouds. Schneider et al. (1989) suggested that the H I clouds in the Leo ring might be primordial, however Bekki et al. (2005) have modelled the Leo Ring and show that tidal debris are very plausible in this example.
Briggs (2005) states that primordial matter does not exist in the form of H I clouds , because all intergalactic clouds are products of their environment. No H I clouds are found yet, unaccompanied by galaxies. In this case the H I is companied by several group members.

Classifying the H I complexes as High Velocity Clouds causes also some problems. If the complexes are HVCs, they are very close to the galaxies, at a distance of ~ 100 kpc from NGC 5033 and within ~ 75 kpc of NGC 5002 and NGC 5033. This is even closer than the distances suggested by de Heij et al. (2002); within 150-200 kpc. Furthermore in most cases the masses are larger than the predicted masses of $10^5 - 10^7 M_\odot$. The determined masses come closer to the masses predicted by Blitz et al. (1999); $\sim 10^7 M_\odot$. However in this scenario the predicted distances of ~ 1 Mpc are out of discussion. What makes it difficult is the large variety of masses and sizes. Some complexes may be build up by smaller clouds, which makes smaller masses possible. However this does not hold for LGG334HI 3, the largest H I complex in the region, where the mass is $\sim 10^8 M_\odot$.
Very recently Westmeier et al. (2004) have found HVCs within 50 kpc of M31. These are small HVCs with a mass of $\sim 10^5 - 10^6 M_\odot$, sometimes connected by bridges. The structures of some complexes in LGG 334 look comparable to the H I clouds found by Westmeier et al. (2004). However in the case of M31 the detected masses are very small, compared with the total mass found in LGG 334 which makes it unlikely that the two cases are the same ($\sim 5 \times 10^6 M_\odot$ against $\sim 2.4 \times 10^8 M_\odot$).
It seems unlikely that the complexes are Dark Matter Clouds, or even a Dark Matter galaxy as found by Minchin et al. (2005) in the Virgo Cluster. To form a Dark galaxy, the cloud should be in dynamic equilibrium, which is not likely with the asymmetric shapes and filaments found in the complexes. Furthermore putative parents for possible tidal debris exist in the neighborhood.

4.1. Tidal Debris

Many dynamical avenues are available to drive tidal evolution in cluster galaxies. The most obvious is the cluster potential itself, particularly for galaxies whose orbit takes them close to the cluster center; e.g. Henriksen & Byrd (1996). In the center of LGG 334 galaxies are close to each other and the crossing time is much smaller than the Hubble time, meaning that interactions between

these galaxies is very likely.
If a diameter of $\sim$ 15 kpc is considered for an average complex and a velocity width of ~ 50 km s^{-1}, an estimate for the dynamical timescale of $\tau_{dyn} = D/\Delta v \approx 2 \cdot 10^8$ year is obtained. This is smaller than the crossing time ($\sim 10^9$ year).
English et al. (2003) have tested the idea that globular clusters form during the interactions and mergers of disk galaxies. Numerical simulations were compared with observations to examine the hypothesis that H I fragments with masses greater than $10^{7\pm1} M_\odot$ are sites of globular cluster formation. With the interaction of galaxies, hydrogen gas is driven from the outer regions of the galaxies into the center of the interacting system. In these reservoirs of hydrogen, star bursts can occur, creating dense star clusters, similar to observed Globular Clusters.
The H I masses of the clouds in LGG 334 are of the same order as the masses predicted by English et al. (2003). Because of the high column densities star formation would be expected, so these clouds should eventually turn into small galaxies or Globular Clusters.

The scenario of tidal debris seems the best explanation for the intergalactic H I. The observations satisfy the scenario presented recently by Bekki et al. (2005) very well. They present a scenario for massive intragroup H I clouds that are the high density parts of large H I rings or arcs. These structures are formed during dynamical interactions of galaxy groups and low surface brightness galaxies (LSB) with extended gas disks. They demonstrate that the tidal field of the group is very efficient at stripping away the outer H I gas of the disk if the gaseous disk of the LSB galaxy extends 2-5 times further than the stellar disk. The original galaxies can remain on their path with an unaffected optical disk, while a stream of H I gas can be formed, orbiting the group center. The model is shown in Fig. 17, after a interaction the stripped H I gas orbits the group center in a stream, finally forming a ring like structure.
The result of such an interaction is a ring-like or arc-like gas cloud, with a very inhomogeneous density distribution ($N_{HI} \sim 1.0 \times 10^{17} - 1.1 \times 10^{20}$ cm^{-2}) and initially no stellar content. If the detection limit for H I gas is not low enough, not the whole cloud can be seen and only the parts of the ring with high densities can be detected. These regions will appear as isolated H I islands near the group center. Star formation can occur in these clouds if the amount of gas in the ring or arc is large enough.
Although a large amount of gas is stripped away from the initial galaxy, the stellar part is not influenced very much by the tidal field of the group. In contrast with the H I, no stellar tails or streams are formed. In this way a gaseous ring can be formed in the center of the group, without stars. It should be highlighted that in this model the original galaxy, from which the ring is formed, lies not within this ring. So at first hand there seems to be no physical connection between the H I ring and the galaxy outside the ring.

In the model, as can also be seen in Fig. 17, the Leo Ring is discussed in great detail, which is very interesting for comparison. The gas in the Leo Ring is isolated from the nearby galaxies. The Ring contains clumps of strong H I emission of a few kiloparsec in diameter. The properties of these clumps are very similar to some of the clouds in LGG 334. They have typical H I masses of $10^7 M_\odot$, reaching a maximum column density of about 4×10^{20} cm^{-2}. The masses of the H I complexes in LGG 334 are of the same order going up to $1.28 \times 10^8 M_\odot$ for LGG334HI 3. In this single cloud the column density reaches 6×10^{20}, but furthermore also the column densities are very comparable.
The scenario of Bekki et al. (2005) seems representative for the situation in group LGG 334. Although there is no ring observed, the features look very similar. Probably only the H I islands are detected, which are the high density parts of this possible ring or arc. The observed column densities are in the same range. Because the detection limit in our observations is $\sim 2.0 \times 10^{18}$ cm^{-2}, it is not ruled out that there is also emission with a column density of $\sim 1.0 \times 10^{17}$ cm^{-2}. There are indications for connections of at least a part of the clouds. Deeper observations are needed to investigate this further and evidence for a ring or arc structure can be revealed.
The situation in group LGG 334 seems however to be more complex than proposed in the model of Bekki et al. (2005). There is not one singular galaxy as described in the scenario, but there are already several galaxies in the neighborhood of the galaxy center. Because direct tails are not detected, it remains unclear, which galaxies actually could have played a role in merging. An interaction of more galaxies is also possible, which probably would distort the shape of a nice ring or arc.
An interaction between NGC 5014 and NGC 5002 is most likely, because these galaxies are mostly disturbed. Furthermore the observed intergalactic H I mass is of the same order as in the galaxies.

4.2. Mass Correlations

There is a strong correlation between the (angular) H I diameter D_{HI}, defined at a surface density of 1 M$_\odot$ pc^{-2} and the optical absorption-corrected diameter $D_{25}^{b,i}$, measured at the 25^{th} mag arcsec^{-2} isophote (Broeils & Rhee, 1997):

$$\log D_{HI} = (1.00 \pm 0.03) \log D_{25}^{b,i} + (0.23 \pm 0.04). \quad (6)$$

There is no obvious correlation of the diameter ratio with type.
Broeils & Rhee (1997) have investigated a large sample of galaxies for H I Mass as a function of H I and optical diameter. The least-squares fits to these data are:

$$\log M_{HI} = (1.96 \pm 0.04) \log D_{HI} + (6.52 \pm 0.06), \quad (7)$$

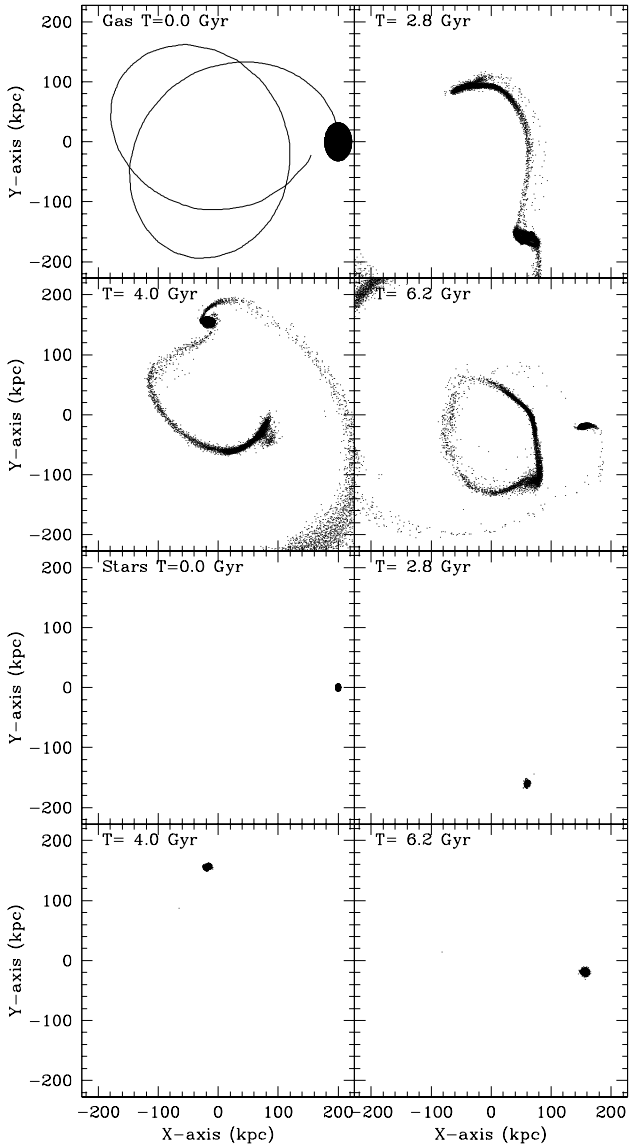

Fig. 17. from Bekki et al. (2005): Morphological evolution of a low surface brightness galaxy in time. The galaxy has an extended H I disk and orbits the center of the group. The four top panels show the gaseous component while the stellar component is shown in the bottom panels. In the upper left panel, the orbital evolution of the galaxy is given. T represents the time that has elapsed since the start of the simulations. In the gas, dense parts can be seen and a giant intragroup H I ring of size ∼200 kpc is formed at $T = 6.2$ Gyr which contains no stars. The constraints of this H I ring are similar to those of the Leo ring (Schneider et al., 1989).

$$\log M_{HI} = (1.95 \pm 0.06) \log D_{25}^{b,i} + (7.00 \pm 0.08) \qquad (8)$$

with $r = 0.98$ and a dispersion of 0.13 dex for the M_{HI} - D_{HI}, and $r = 0.94$ and 0.19 dex for the M_{HI} - $D_{25}^{b,i}$ relation. These least-squares fits are plotted in Fig 18 with the measured values for the group members in LGG 334. In Table 6 the diameters of the group members are given and the dispersions from the correlations as determined by Broeils & Rhee (1997). The optical diameters are taken from HyperLeda, at the 25^{th} mag arcsec^{-2} isophote. The H I diameters are determined at a surface density of 1 $M_\odot$ pc^{-2}. In Fig. 18 the left purple triangle represents the H I of NGC 5002 with its own H I mass and the total intergalactic H I mass added. In this case it is assumed that NGC 5002 is the host galaxy and that all the intergalactic gas originally comes from this galaxy. The right triangle represents twice the optical diameter of NGC 5002 and the same mass as the other triangle. This is because the model of Bekki et al. (2005) predicts that the original H I disc is at least twice as large as the optical diameter.

The group members fit the predicted correlations very well. With the exception of UGC 8303, the galaxies have an indication to be a little bit mass deficient, however in all cases the deviation is smaller than the given dispersions, of respectively 0.13 and 0.19 for the H I and optical diameter.

Although there is no obvious mass deficiency, it is possible that the intergalactic H I gas comes from NGC 5002. When the found intergalactic H I mass is added to the mass of NGC 5002 the dispersion is getting large, and the galaxy would have been gas rich. However in the model of Bekki et al. (2005), H I diameters are predicted, larger than two times the optical disk. So when the same mass is taken as before, with twice the optical diameter, the galaxy still is a little bit gas rich, indicating that the original gas disk could have been larger than twice the optical disk while the correlation of Broeils & Rhee (1997) still holds.

Using these estimates, a scenario as described by Bekki et al. (2005), with NGC 5002 as host galaxy is possible. In the model of Bekki et al. (2005), about 43 per cent of the initial H I is stripped from the original galaxy. If NGC 5002 is considered as the parent galaxy, about 40 per cent of the H I gas would have been stripped.

A scenario, where NGC 5002 has interacted with another galaxy, or the group potential is certainly not contradicted by the known mass correlations and seems most likely.

Another indication for NGC 5002 being the host galaxy is the radial velocity of the galaxy. As can be seen from the global profiles, the radial velocities of almost all the H I complexes are in the range of the profile of NGC 5002. The mass of NGC 5014 is of the same order as the mass of the complexes and also the radial velocity is of the same order. This indicates, that this group member may also play an important role in the interaction. Because of the large plume and the connection with LGG334HI 12 it seems that gas is accreting into the galaxy; also the polar ring could be explained as a result of the interaction.

4.3. Polar Ring Galaxy NGC 5014

As well as the optical, but especially the H I data of NGC 5014 show a ring, which is tilted with respect to the main disk. The fact that the ring is not exactly polar, might be an indication that the ring has formed recently and is not stable. Furthermore, the ring structure is smaller than the main disk, therefore it is probably an

Galaxy	H I diameter	optical diameter	H I dispersion	optical dispersion
NGC 5033	69.3 kpc	46.6 kpc	-0.12	-0.25
NGC 5014	13.7 kpc	7.2 kpc	-0.06	+0.01
NGC 5002	12.2 kpc	7.2 kpc	-0.08	-0.11
UGC 8303	14.9 kpc	9.6 kpc	+0.10	+0.01
NGC 5002, with D_{HI} and added mass.				
NGC 5002	12.2 kpc		+0.17	
NGC 5002, with twice $D_{25}^{b,i}$ and added mass.				
NGC 5002	14.4 kpc		+0.03	

Table 6. Group members and diameters. The last two columns give the dispersions in Fig. 18, a negative dispersion is an indication for a gas poor galaxy and a positive dispersion is an indication for a gas rich galaxy.

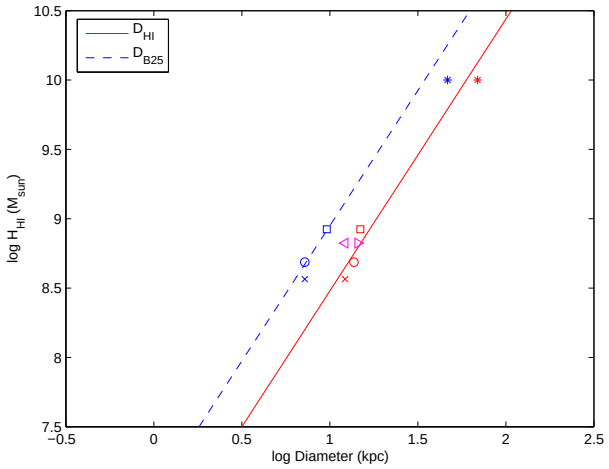

Fig. 18. Correlation between H I mass and linear H I diameter (red line) and linear optical diameter (blue line) from Broeils & Rhee (1997). Stars represent the H I (red) and optical (blue) diameter of NGC 5033. The squares represent UGC 8303, circles NGC 5014 and crosses NGC 5002. The left triangle is the H I diameter of NGC 5002 with its own H I mass with the found intergalactic H I mass added. The right triangle is twice the optical diameter of NGC 5002 and its own H I mass with the found intergalactic H I mass added.

internal structure. Other examples of polar ring galaxies with small rings or rings which are not perpendicular to the main disk can be found in Whitmore et al. (1990). This ring is gas rich, while the host galaxy is almost depleted of gas, which indeed is an indication for a polar ring.

For this reason it is interesting to try to give constraints on how this polar ring is formed and how it is related to the other H I complexes.

In our observations, the accretion scenario is most likely for the formation of the polar ring. There is a lot of H I gas, which is assumed to be tidal. No remnants of a galaxy can be seen that would indicate a merging scenario. This result is consistent with other observations. Even if the merging scenario is rather robust, most polar ring galaxies are shown to be the result of tidal gas accretion (Bournaud & Combes, 2003).

The polar ring can be an extra argument for the tidal interaction scenario. The large amount of intergalactic gas and the formation of a polar ring cannot be an accident and we think that they have the same origin.

A question would be why we do not see scenarios as observed here in many other group. Probably the conditions are very unique. A galaxy is needed with a very extended H I disk in the center of a group. Comparable H I structures cannot be seen around High Surface Brightness galaxies, because here tidal stripping is much less efficient. Around galaxies with a compact H I disk, most of the gas would be consumed by star formation due to the initial high gas densities in the disks.

5. Summary and Conclusion

The central part of LGG 334 is observed in H I with the WSRT and optical with the MDM Hiltner 2.4m telescope. These observations are deeper than previous observations and provide much interesting information. Four group members are identified and eight intergalactic H I complexes are found without an optical counterpart to a 1σ surface brightness limet of 27.6 mag arcsec^{-1} in the B-band and 27.2 mag arcsec^{-1} in the R-band. The observed H I masses of these complexes range from $1.44 \cdot 10^6 M_\odot$ to $1.28 \cdot 10^8 M_\odot$.

The observations are inconsistent with any theory of High Velocity Clouds and also cannot be compared with other observations of possible HVCs. The clouds are to close to the galaxies to fulfill the theory predicted by Blitz et al. (1999). Although there is a trend that HVCs are believed to be closer around galaxies, the found complexes are too large to support the scenarios from e.g. de Heij et al. (2002) and Braun & Burton (1999). Also a primordial or Cold Dark Matter origin are not likely.

We hypothesize that the intergalactic H I gas has a tidal origin. The gas is depleted from one or more of the group members by interaction in the group center. Probably NGC 5002 and NGC 5014 have been involved in this interaction. NGC 5002 has interacted with the potential of the group or another galaxy and a part of the H I gas is captured by NGC 5014, or both galaxies have interacted, where a part of the depleted gas is captured back by NGC 5014. The captured gas in this event has caused the polar ring in NGC 5014.

A model by Bekki et al. (2005) indicates what could have happened in this group. This model shows how rings or arcs of H I gas can develop without stars, as a result of interaction of a low surface brightness galaxy with the potential of a group of galaxies. This scenario is not contradicted, by the discussed mass correlations.

Stars would be expected in the dense parts of the H I complexes because of the local high column densities. Although no optical emission has been found, star formation is very likely, where the column density is higher than $\sim 1 \cdot 10^{20}$ cm^{-2}. Hα observations are needed to investigate this. Furthermore it would be interesting to look for other elements in the H I complexes. When other, more massive elements are found than hydrogen, it would be a proof that the gas comes from galaxies.

Acknowledgements. We would like to thank Jelte de Jong for making the optical observations, also on the turn of the year from 2002 to 2003 and Tom Oosterloo for giving useful help and comments on the reduction of the H I data. The Westerbork Synthesis Radio Telescope is operated by the ASTRON (Netherlands Foundation for Research in Astronomy) with support from the Netherlands Foundation for Scientific Research (NWO). We made use of the data from the Lyon Extragalactic Database (LEDA; http://leda.univ-lyon1.fr/) and the NASA/IPAC Extragalactic Database (NED; http://nedwww.ipac.caltech.edu/) which is operated by the Jet Propulsion Laboratory, California Institute of Technology, under contract with the National Auronautics and Space Administration.

References

Barnes, D. G. & Webster, R. L. 2001, MNRAS, 324, 859
Bekki, K. 1998, ApJ, 499, 635
Bekki, K., Koribalski, B. S., Ryder, S. D., & Couch, W. J. 2005, MNRAS, 357, L21
Blitz, L., Spergel, D. N., Teuben, P. J., Hartmann, D., & Burton, W. B. 1999, ApJ, 514, 818
Bothun, G. D., Impey, C. D., Malin, D. F., & Mould, J. R. 1987, AJ, 94, 23
Bournaud, F. & Combes, F. 2003, A&A, 401, 817
Braun, R. & Burton, W. B. 1999, A&A, 341, 437
Briggs, D. 1995, Ph.D. Thesis, New Mexico Inst. Mining Tech
Briggs, F. H. 2005, astro-ph/0502306
Broeils, A. H. & Rhee, M.-H. 1997, A&A, 324, 877
de Heij, V., Braun, R., & Burton, W. B. 2002, A&A, 392, 417
English, J., Norris, R. P., Freeman, K. C., & Booth, R. S. 2003, AJ, 125, 1134
Freeman, K. C. 1970, ApJ, 160, 811
Garcia, A. M. 1993, A&AS, 100, 47
Henriksen, M. & Byrd, G. 1996, ApJ, 459, 82
Hibbard, J. E., van Gorkom, J. H., Rupen, M. P., & Schiminovich, D. 2001, in Astronomical Society of the Pacific Conference Series, 657–+
Landolt, A. U. 1992, AJ, 104, 340
Minchin, R., Davies, J., Disney, M., Boyce, P., Garcia, D., Jordan, J., Kilborn, V., Lang, R., Roberts, S., Sabatini, S., & van Driel, W. 2005, astro-ph/0502312
Muller, C. A., Oort, J. H., & Raimond, E. 1963, C.R. Acad.Sci.Paris, 257, 1661
Noordermeer, E., van der Hulst, J. M., Sancisi, R., Swaters, R. A., & van Albada, T. S. 2005, A&A, in prep
Reshetnikov, V. & Sotnikova, N. 1997, A&A, 325, 933
Ryan-Weber, E., Webster, R., & Bekki, K. 2003, in ASSL Vol. 281: The IGM/Galaxy Connection. The Distribution of Baryons at z=0, 223–+
Sault, R. J., Teuben, P. J., & Wright, M. C. H. 1995, in Astronomical Society of the Pacific Conference Series, 433–+
Schneider, S. E., Skrutskie, M. F., Hacking, P. B., Young, J. S., Dickman, R. L., Claussen, M. J., Salpeter, E. E., Houck, J. R., Terzian, Y., Lewis, B. M., & Shure, M. A. 1989, AJ, 97, 666
Schwarz, U. J. 1978, A&A, 65, 345
Swaters, R. A., van Albada, T. S., van der Hulst, J. M., & Sancisi, R. 2002, A&A, 390, 829
Thean, A. H. C., Mundell, C. G., Pedlar, A., & Nicholson, R. A. 1997, MNRAS, 290, 15
Toomre, A. & Toomre, J. 1972, ApJ, 178, 623
van der Hulst, J. M., Terlouw, J. P., Begeman, K. G., Zwitser, W., & Roelfsema, P. R. 1992, in in ASP Conf. Ser. 25: Astronomical Data Analysis Software and Systems I, 131
Vogelaar, M. G. R. & Terlouw, J. P. 2001, in in ASP Conf. Ser. 238: Astronomical Data Analysis Software and Systems X, 358
Wakker, B. P. & van Woerden, H. 1997, ARA&A, 35, 217
Westmeier, T., Bruens, C., & Kerp, J. 2004, astro
Whitmore, B. C., Lucas, R. A., McElroy, D. B., Steiman-Cameron, T. Y., Sackett, P. D., & Olling, R. P. 1990, AJ, 100, 1489
Yang, B., Zhu, J., & Song, Y. 2002, Chinese Journal of Astronony and Astrophysics, 2, 474
Zucker, D. B., Kniazev, A. Y., Bell, E. F., Martínez-Delgado, D., Grebel, E. K., Rix, H., Rockosi, C. M., Holtzman, J. A., Walterbos, R. A. M., Annis, J., York, D. G., Ivezić, Ž., Brinkmann, J., Brewington, H., Harvanek, M., Hennessy, G., Kleinman, S. J., Krzesinski, J., Long, D., Newman, P. R., Nitta, A., & Snedden, S. A. 2004, ApJ Lett., 612, L121
Zwaan, M. A. 2001, MNRAS, 325, 1142